Effect of local and remote sources and new particle formation events on the activation properties of cloud condensation nuclei in the Brazilian megacity of São Paulo.

Carlos Eduardo Souto-Oliveira[1,2], Maria de Fátima Andrade[3], Prashant Kumar[4,5], Fábio Juliano da Silva Lopes[3,6], Marly Babinski[1], Eduardo Landulfo[6].

[1]Geocronological Research Centre, Institute of Geosciences, University of São Paulo, São Paulo, 05508-080, Brazil
[2]Chemistry Research Centre, UNIFIEO, São Paulo, 06018-903, Brazil
[3]Department of Atmospheric Sciences, Institute of Astronomy, Geophysics and Atmospheric Sciences, University of Sao Paulo, Sao Paulo, 05508-090, Brazil
[4]Department of Civil and Environmental Engineering, Faculty of Engineering and Physical Sciences (FEPS), University of Surrey, Guilford GU2 7XH, United Kingdom
[5]Environmental Flow (EnFlo) Research Centre, Faculty of Engineering and Physical Sciences, University of Surrey, Guildford GU2 7XH, United Kingdom
[6]Nuclear and Energy Research Institute, IPEN-CNEN, Centre for Laser and Applications (CLA), São Paulo, 05508-970, Brasil

Correspondence to: Carlos Eduardo Souto-Oliveira (carlos.edu.oliveira@usp.br)

Abstract. Atmospheric aerosol is the most important source of cloud condensation nuclei (CCN). Microphysics and chemical composition of aerosols can affect cloud development and precipitation process. Only a few studies in Latin American have reported the impact of urban aerosol on CCN activation parameters such as activated ratio (AR) and activation diameter (D_{act}). Sao Paulo Metropolitan Area (SPMA) is the biggest megacity of South America with over 20 million inhabitants. This is the first study in a megacity on South America to assess the impact of remote sources and new particle formation (NPF) events on CCN activation properties. The measurements were conducted at São Paulo city from August to September 2014. The CCN were measured within the 0.2–1.0% range of supersaturation, simultaneously with particle number concentration (PNC) and distribution (PND), trace elemental concentrations (TEC) and black carbon (BC). The NPF events were identified during 35% of the sampling days. Combination of TEC and BC associated with aerosol profile from Lidar analysis and Hysplit trajectories allowed to identify sea-salt and biomass burning contribution from remote regions as 28% and 21% of total number of days, respectively. The AR and D_{act} parameters presented a clearly different pattern for diurnal and nocturnal periods. The diurnal periods presented lower CCN activation than the nocturnal durations and this pattern was found to be associated mainly with local vehicular traffic emissions. NPF events showed a negative feedback to CCN activation. Weak effects of sea-salt and biomass burning aerosols could be observed on activation

Atmospheric
Chemistry
and Physics
Discussions

parameters as sea-salt showed a positive feedback. The results of this study show that particulate matter from local traffic emissions has the main effect on activation parameters compared with remote sources.

5 **1 Introduction**

Atmospheric aerosol has been the focus of numerous studies due to their adverse effects on public health and climate (Heal et al., 2012). Aerosol particles are a significant source of cloud condensation nuclei (CCN). Through their microphysics and chemical composition, aerosol particles can affect cloud development and precipitation process. The high concentration of CCN in the air favor clouds formation with small droplets, which can lead to suppression of precipitation in shallow and

10 short-lived clouds (Andreae and Rosenfeld, 2008). Such phenomena have been observed at different places. A study carried out at Brazilian Amazonian forest showed reduction of precipitation due to scavenging during vegetation burning events (smoky clouds) compared with cloud formed under clean (blue and green ocean) air masses. The smoky clouds were formed in higher altitudes (>4 km) due to smaller droplets size, and produced hydrometeors and isolated intense showers and thunderstorms (Andreae et. al., 2004; Freud et al., 2008).

15 The CCN activation properties can be estimated by parameters such as activated ratio (AR) and activation diameter (D_{act}). These parameters have been employed by several studies representing different locations of the world for verifying the efficiency of aerosol particles to act as CCN. The variability of these parameters is dependent of size and chemical composition of particles. In general, D_{act} is more sensitive to chemical composition of aerosol while AR responds to size and chemical composition. Normally large particles, inorganic salt and polar organic molecules are more hygroscopic than

20 smaller or non-polar ones (e.g. hydrocarbons). Some studies have reported that aerosol from polluted air masses (e.g. urban, fresh traffic, biomass burning) are less efficient for CCN activation (>D_{act} and <AR) than non-polluted air masses (e.g. forest, marine) (Frank et al., 2006; Andreae and Rosenfeld, 2008; Quinn et al, 2008; Furutani et al., 2008; Bulkart et al., 2011; Deng et al., 2013; Leng et al., 2013; Paramonov et al., 2013). However, some studies carried out at different locations and environmental conditions have demonstrated that aged polluted aerosols presented CCN activation properties similar to

25 non-polluted or even marine environment (Peng et al., 2014). These observations are supported by the growth of particles, atmosphere processing of non-soluble organics and mixture with more hygroscope compounds such as sulphate, nitrate, organic acids (Andreae et la., 2004; McFiggans et al., 2006; Quinn et al, 2008; Furutani et al., 2008; Dusek et al., 2010; Bougiatioti et al., 2011; Zhang et al., 2014).

Aerosols are originated both in primary and secondary process. Primary aerosols are emitted to the atmosphere directly by

30 anthropogenic and natural sources. On the other hand, secondary particles are formed in the atmosphere by nucleation of non- or low-volatile gases with inorganic and organic compounds, followed by growth to larger particles (Holmes et al., 2007). The new particle formation (NPF) directly affects particle number concentrations (PNC) and size distributions (PND)

and optical properties of aerosols, besides impacting CCN and cloud properties. These events have been recently studied in different environments (urban, coastal, forest) (Kulmala et al., 2004; Dal Maso et al., 2005; Backman et al., 2012; Betha et al., 2013; Peng et al., 2014; Wei Nie et al., 2014; Junlin An et al., 2015; Sorribas et al., 2015; Kumar et al., 2014). However, only a small number of works have evaluated the effect of NPF on CCN properties (Dusek et al., 2010; Yue et al.,

5   2011;Sihto et al., 2011; Paramonov et al., 2013).

The Sao Paulo Metropolitan Area (SPMA) is the biggest megacity of South America with over 20 million inhabitants. Thus, the SPMA represents an important city for global scale atmosphere. This metropolitan area has more than 7 million of vehicles, many industries and construction activities as the main sources of particles (IBGE, 2014). To date, there is only one study performed for measuring and modeling the CCN in the SPMA (Almeida et al., 2014). In general, there are only limited

10   studies which have reported CCN, PNC and PND measurements and the effects on atmosphere in Latin American compared with those in European and North American cities (IPCC, 2013).

The aim of this paper is to evaluate CCN activation properties under local and remote sources, as well NPF events. We measured CCN simultaneously with PNC, PND, black carbon (BC) and trace-elemental concentration (TEC). PND contour plots were constructed to identify and classify NPF events. Light detection and ranging (Lidar) analyses and Hysplit

15   trajectories were combined with TEC and BC size distributions to identify air mass from local and remote sources in the SPMA. The effect of these air masses and NPF events on CCN activation properties was evaluated. In the best of our knowledge, this is the first study in any megacity of South America to evaluate the effect of remote sources and NPF events on CCN activation properties.

20

2 Methodology

2.1 Site description and meteorological data

The SPMA (23.5^{o}Sand 46.6^{o}W) is an urban region spread over a surface area of 7946 km^2, which is situated in the southwest region of Brazil (fig. 1). With over 20 million inhabitants, the SMPA is the biggest megacity in Latin America and rank

25   fourth among all megacities in the world. The SPMA is situated on a sedimentary basin of Sao Paulo as a main valley (the Tiete River) that has a mean elevation of 720 m. The Atlantic Ocean is about 45 km from SPMA in the southeast direction.

The measurements were conducted on the rooftop of Astronomy, Geophysics and Atmospheric Sciences Institute (IAG) located in the University of Sao Paulo main campus (USP, 23.56ºS and 46.73ºW), which is situated on west region of Sao Paulo city. There is a main road (Marginal Pinheiros and Tietê) around 1 and 3 km northeast and north respectively from the

30   sampling site. These roads have high traffic density (i.e. 8000 automobiles, 90 buses, 220 trucks and 1500 motorcycles per hour) during the day time (0700 - 1900 h; local time). During the night, traffic volume is less than half to what is noted during the daytime and is dominated by heavy-duty vehicles (mainly trucks). Other important source of particles in the

SMPA area is construction sites inside and outside the USP campus and a cement industry about 2 km to the west. The major industrial areas are located approximately 45 km (Cubatão) and 30 km (Maua) southeast; Cubatão industrial city is in a coastal region (fig. 1).

2.2 Measurements of CCN

5   The CCN was measured by a single-column continuous-flow stream-wise thermal gradient CCN chamber (DMT CCNC-100). The supersaturated water vapour is generated inside the column centre line (0.9 mm radius, 360 mm long and wall thickness of 8 mm), which is controlled by the gradient temperature. When supersaturation (SS) generated is larger than critical supersaturation (SC), the particle grows to critical diameter activation; particle size can increase to cloud droplets after this point. After activated particles leaves the column chamber are counted by an optical particle counter (OPC) in the
10   0.75-10 µm size range, which employ standard light scattering technique (Roberts and Nenes, 2005).

All samples were collected continuously between 19 August and 03 September 2014. CCN instrument operated at flow rate 0.5 L min^{-1} with variable SS concentrations (0.2, 0.4, 0.6, 0.8 and 1.0 %). Each cycle (~25 min) corresponds to each SS value measurements for 5 minutes, data used in analysis consider only supersaturation steady state.

2.3 Measurements of size-resolved particles

15   The measurements of PND and PNC were made using a Differential Mobility Particle Size (DMPS, model3936). The DMPS consists of a Differential Particle Analyser (DMA, model 3080) and a Condensation Particle Counter (CPC, TSI model 3010). The DMA separates particles according to their electrical mobility and the particles that pass DMA column are counted by CPC (Kumar et al., 2010). In CPC, particles increase to droplets by condensation of alcohol vapour and then counted by laser beam.

20   The aerosol size distribution was measured in the 10 to 450 nm size range, scanning particles in 22 diameter size bins, with a 5 minutes time resolution. The gas sample and sheath flow were 1.0 and 6.0 L min-1, respectively.

The DMPS particle concentrations have been found to show undercounting of particles during ambient measurements, mainly due to lower DMA transfer probability or deviation for sampling and sheath flow rates. Additionally, PNCs were measured until 450 nm only, so AR values can be overestimated. A correction factor of 1.3 was applied to the whole data in
25   order to correct undercounting of measured PNC and overestimation of AR. This factor was obtained by linear fitting of scatter plot (CCN versus CN) of data with AR>1 values. In order to verify the factor assurance, the PNC distribution was integrated until 1.0 µm, which represent most of total PNC. Calculated factor to obtain PNC until 1.0 µm was 1.15. Almeida et al. (2014) used the same DMPS equipment and considered a factor of 1.12 to correct similar undercounting of PNCs.

2.4   Measurements of BC and TEC species

30   Micro-orifice Uniform Deposit Impactor (MOUDI) was used to collect particles of <0.056, 0.05618, 0.1, 0.18, 0.32, 0.56, 1.0, 1.8, 3.2, 5.6 and 10 µm. The MOUDI selects particles by the size of orifices and operates with the sampling air flow of

30 l min^{-1}. In each stage, the particles larger than the size of micro-orifice were collected on polycarbonate filter (Whatman, 47 mm diameter, 8 µm pore size). The sampling interval was 12h, which comprehends day (0700-1900 h) and night (1900-0700 h) periods. After collection, filters were stored in temperature and humidity controlled room until their analysis were performed.

5   The aerosol mass concentrations were measured gravimetrically before and after the sampling; the filters were weighed on a microbalance that has 1 µg readability (Mettler-Toledo, Columbus, OH, USA). Elemental concentrations were determined by Energy Dispersive X-ray Fluorescence Spectrometer (EDX 700; Shimadzu Corporation, Analytical Instruments Division, Tokyo, Japan). The spectrometer operates at 5–50 kV and 1–1,000 µA, using a low-power Rh-target tube. The elemental characteristic raio-X radiation emitted from aerosol sample are detected by Si(Li) detector. The obtained spectra were
10   processed and quantified by WinQXAS program, available from the website of the International Atomic Energy Agency (http://www. iaea.org/OurWork/ST/NA/NAAL/pci/ins/xrf/pciXRFdown.php).

BC was measured by optical reflectance with a smoke stain reflectometer (model 43D; Diffusion Systems Ltd, London, UK). The visible light were emitted from tungsten lamp and reflected radiation detected. The empirical calibration curve that converts from reflected signal to BC concentrations was obtained. The light-absorbing by carbonaceous fraction present in
15   atmospheric aerosol are correlated with elemental carbon.

2.5   Monitoring of gases and UV radiation

To verify the importance of some gaseous concentrations (SO$_2$, O$_3$, NO and NO$_x$) and UV radiation during the days of NPF events, hourly values of the compounds measured by Environmental Protection Agency of Sao Paulo (CETESB) were considered. The O$_3$ and UV radiation were measured in a CETESB station located inside USP (Ipen), which is about 500m
20   away from the IAG. The sulphur dioxide (SO$_2$), ozone (O$_3$), nitrogen monoxide (NO) and nitrogen oxides (NO$_x$) data were obtained from four CETESB station located outside the USP. These stations are located at 7 Km northwest (Osasco), 5 Km north (Marginal Pinheiros), 10 Km southeast (Congonhas) and 5 Km southwest (Taboão da Serra) from USP. These four stations were chosen by the predominance of wind direction.

2.6   Lidar and trajectory analyses

25   A Raman lidar system (MSP-lidar I) installed at the Nuclear and Energy Research Institute (IPEN) was employed to measure independently profiles of the particle extinction and backscatter coefficients and, thus, the particle extinction-to-backscatter ratio at 532 and 355 nm, respectively. It comprises a commercial Nd:YAG laser operating at 355 nm and 532 nm. The output energy per pulse is 400 mJ for 532 nm and 230 mJ for 355 nm, at a repetition rate of 10 Hz and pulse duration of 5 ns. The light beam is expanded by a factor of 5 in order to reduce the divergence of the expanded beam to less than 0.5 mrad. The
30   laser beam is vertically directed to the atmosphere and the backscattered radiation is collected with a coaxial Newtonian telescope that has a primary mirror diameter of 300 mm and a focal length of 1.5 m. The receiver field of view is set to 0.1 mrad, providing a complete overlap between the laser beam and the telescope field of view at altitudes close to 300 m above

the lidar system. After separating and passing the respective interference filters, the photons elastically backscattered at the 355 and 532 nm wavelength and the photons inelastically (Raman) scattered by nitrogen molecules at are detected 387 nm and 607 nm by photomultiplier tubes (PMTs, Hamamatsu type R9880U-110). The bandwidth of the filters in 355 nm and 532 nm are 1 nm while 387 and 607 nm channels are 0.25 nm. A transient digitizer operating in analog and photon counting

5 modes recorded data in 12-bit resolution. Data are averaged every 2 min, with a typical height resolution of 7.5 m. Since 2008 the MSP-Lidar I system is at SPU-Station, belonging to LALINET (http://lalinet.org), a federative coordinated lidar network focused on the vertically-resolved monitoring of the particle optical properties distribution over Latin America (Rascado et al., 2015, Rascado et al., 2016).

Air masses trajectories are computed using GDAS (Global Data Assimilation System), an operational system from the

10 National Weather Service's National Centers for Environmental Prediction (NCEP). The GDAS is used as input in the Hybrid Single Particle Lagrangian Integrated Trajectory Model (HYSPLIT – Version 4.8). It is selected forward or backward trajectories according to the case and chosen the model vertical velocity option (Draxler and Hass, 1998). These trajectories provide the source of air masses arriving in São Paulo at different levels (altitudes) in a preset time interval, using as starting point the coordinates of IAG, where the instruments are installed.

15 **3 Results and discussion**

3.1 Meteorology, CCNC and PNC during the measurements

This study was conducted in winter season, which represent mostly dry climate. However, three rain events were observed during the evaluated period. Table 1 presents the average values of meteorological parameters, PNC and CCN data for evaluated period. Days 7 and 8 had the lowest mean temperature while day 5 presented the highest; major temperature

20 variation (16.1°C) was seen on the 11th day. The mean relative humidity (RH) was higher than 70 % for all days, except for days 4 and 5 with means of 62 and 58 %, respectively. The greatest variation of RH occurred during days 3, 4 and 11. The precipitations were observed in day 6 in the morning and during days 11 and 13 at night (Fig. 2a).

Total PNC (9-1000 nm) varied between 1347 and 35508 cm^{-3}, with a mean of 11634 ± 3077cm^{-3}. Our PNC mean value is higher than those observed in Vienna (7300 cm^{-3}) and lower than measured by Backman et al.(2012) as 23500±1040 cm^{-3}

25 and Almeida et al.(2014) as 12813±5350 cm^{-3} in Sao Paulo. The measurements in Vienna presented a greater variability (with minimum and maximum being 910 and 51600 cm^{-3}, respectively), and the lower concentrations were associated with frontal passages of air masses (Burkart et al., 2011).

The peak diameter observed, calculated by PND mode, was less than 100 nm and presented a mean value of about 55 nm for all days. The highest mean peak diameter (92 nm) was observed on day 6 while the lowest diameter was 29 nm on day 14,

30 characterizing Aitken and nucleation modes respectively (Kumar et al., 2011). The particle size distribution and NPF events are presented in the Section 3.2.

Atmospheric
Chemistry
and Physics
Discussions

CCN concentrations were measured at five different SS levels (0.2, 0.4, 0.6, 0.8 and 1.0%). As expected, the CCN increase with supersaturation (SS) condition (Table 1 and Fig. 1b). For SS=0.2%, minimal and maximum diurnal concentrations were 12 and 10596 cm^{-3}, respectively, with a mean of 1987 ± 942 cm^{-3}. For SS=1.0%, the concentrations varied between 206 and 12761 cm^{-3} with a mean of 3996 ± 1572 cm^{-3}.

5 The CCN values obtained in this study were slightly higher than those observed in Sao Paulo during October 2012 (Almeida et al., 2014), which presented a mean of 1090±328 cm^{-3} to SS=0.23% and 3570±1695 cm^{-3} to SS=1.13%. Our CCN values are lower than those found in Shanghai (4500 cm^{-3} at SS=0.2%, 5700 cm^{-3} at SS=0.4%, 7000 cm^{-3} at SS=0.6%, 7800 cm^{-3} at SS=0.8%, and 8200 cm^{-3} at SS=1.0%), west coast of Korea (5292 cm^{-3} at SS=1.0%) and Beijing (6000 cm^{-3} at SS=0.17%) (Baumgardner et al., 2004; Yum et al., 2005; Deng et al., 2011; Leng et al., 2013). However, similar values were reported in

10 Mexico city (3000 cm-3 at SS=0.5%) but are higher than those observed in Vienna (820 cm^{-3} at SS=0.5%) and Ireland (208-346 cm^{-3} at SS=0.5%), (Burkart et al., 2011; Reade et al., 2006).

Figure 2 shows the variability of meteorological parameters (temperature, RH and precipitation), CCN and PCN data variability during the studied period. The highest PNCs were observed during rush hour (0700-1800 h) while the lower concentrations occurred at night, (Fig. 2b).The increase in PNCs during rush hours is mostly associated with vehicular traffic

15 emissions. The CCN peaks showed opposite behaviour in relation to PNC, where the higher concentrations were observed at night and at afternoon. These observations are further discussed in Section 3.4.

The precipitation period was characterized by lower PNC and CCN concentrations, as expected. In order to eliminate rain interference on the CCN and PNC data, the periods with rain were excluded of analysis.

3.2 Diurnal PND variability and NPF events

20 This section discusses the identification of NPF events associated with meteorological and chemical conditions, together with some characteristics of hourly distributed NPF classes and the PNDs.

Figure 3a shows diurnal variability of UV radiation intensity, SO_2, O_3, NO and NO_x concentrations. The gaseous concentrations measured at the four CETESB stations were selected according to the prevailing wind directions. UV presented lower intensity during the days 6 and 9, while all other days had high UV intensities (~30 W m^{-2}). The days 1, 2, 4,

25 5, 12, 13 and 14 showed higher O_3 concentrations (80 to 100 μg m^{-3}) compared with days 4, 5, 6, 12 and 14 that had the major NO and NO_x concentrations (100 to 300 ppb). During these days, the peak of NO_x occurred between 0600 and 1100 h, which were associated with vehicular traffic during the first rush hour (0700 to 1000 h). On the day 12, high NO_x and NO concentration (100 to 280 ppb) were observed for the whole day. Figure 3a clearly shows NO_x peaks that occurred before higher O_3 concentrations. This behaviour is expected considering the reaction between NO_x and volatile organic compounds

30 (VOC's) in presence of UV radiation to generate O_3. The ratios of NO_x and VOC's to produce O_3 are demonstrated by O_3 isopleths plot (Finlayson-Pitts and Pitts, 1999; Seinfield and Pandis, 2006).

The presence of O_3, hydroxyl radical (OH) and nitrate radical (NO_3) are fundamental to initiate and maintain photochemical reactions. These reactions yield degradation of VOCs, which produce low volatile species that lead to the formation of

Atmospheric
Chemistry
and Physics
Discussions

secondary organic aerosol (SOA). The addition of polar functional group during oxidation reactions has effect on vapour pressure and polarity of product, which contributes to the SOA chemical composition. The SOA represent a great fraction of aerosol (Kroll and Seinfield, 2008 and references therein).

Some studies have demonstrated the dependence of SOA yield and composition in relation to NO_x concentrations. The

5 oxidation of hydrocarbons and simple aromatics are promoted by NO_x species. The great yield of SOA are related with oxidation of large alkanes (>C12) in presence of high concentrations of NO (Ng et al., 2007; Lim and Ziemann, 2005; Kroll and Seinfield, 2008).

The NO_x values represent the sum of NO and NO_2 concentrations, which are mainly formed by fuel burning at high temperatures in motors and industrial boilers. Figure 3a shows the diurnal variation of NO_x and NO concentrations (denoted

10 by closed and open squares, respectively), which were observed for most days with intermediate concentrations (10 to 40 ppb). The large concentrations of these species were measured only during the days 4, 5, 12 and 14. However, high concentrations dominated the days 12 and 14. During these days, it was observed major nucleation burst, which correspond to occurrence of NPF events, as discussed below in figure 3b. Such observation suggests a significant SOA production and consequent contribution for the NPF. Moreover, O_3 concentrations and UV intensity had great contribution for the

15 photochemical process and SOA production. However, nucleation burst was not observed during the other days as were seen on days 12 and 14. Our findings are in agreement with previous studies that correlate SOA formation with NO_x concentration, for example, SOA contributes to the nucleation and particle growth (Kroll and Seinfield, 2008 and references in).

The main wind direction during the days 12 to 14 were from north and east (fig. 3b), which is expected to carry emissions

20 from the main roads, Marginal Pinheiros and Tietê, that were located at a distance of about 1 to 4 km respectively and are an important source of NO_x. On most days, winds came from south and southeast direction, which contains many roads and two important industrial areas (fig. 1). The wind speed was more intense (4 to 5 m s^{-1}) during days 8, 9, 11, 12 and 14, while wind speeds were lower on the other days.

Recent studies have demonstrated the importance of sulphuric acid (H_2SO_4) to the nucleation and particle growth (Holmes,

25 2007; Yue et al., 2010; Backman et al., 2012). The main mechanisms of NPF have been proposed by binary nucleation with H_2SO_4-H_2O and ternary nucleation with H_2SO_4-H_2O-NH_3 (Kulmala and Laaksonen, 1990, Nepari et al., 2002; Merikanto et al., 2007). Although, VOCs play a significant role for NPF events in the atmosphere (Zhang et al., 2004, 2009), the H_2SO_4 precursor is SO_2 gas, emitted mainly by industrial activities and diesel vehicles.

SO_2 concentrations measured at CETESB stations were plotted according to wind direction in order to represent air masses

30 that arrived to the measurement site (USP) (Fig. 3a). The major concentrations of SO_2 are associated with winds from southeast direction (Congonhas), while winds from north direction presented lower concentrations (Fig. 1a). In addition to the vehicular traffic of main roads, there are two large industrial areas in the southeast direction, which represent important source of SO_2. The SO_2 transport from industrial areas is supported by some studies, which showed that marine air masses

Atmospheric
Chemistry
and Physics
Discussions

and industrial emissions from Cubatão reached the São Paulo city. The sea salt transport is further discussed in section 3.3, based on the chemical and trajectory analyses.

Figure 3c shows PND variability along evaluated days. The diurnal peak concentrations for most days were observed during the rush hour (0700 to 1900 h) in the diameters between 25 and 100 nm (Aitken mode). Diurnal higher concentrations for the

5   days 1, 12 and 14, of particle with diameters lower than 25 nm (nucleation mode) occurred close to noon period. The day 12 presented the major peak concentrations in all the evaluated period.

In order to identify NPF events, we adopted the following requirements described by Dal Maso et al.(2005), extensively employed by other studies (Backman et al., 2012; Betha et al., 2013; Ma and Birmili, 2015): (i) a distinctly new mode of particles (nucleation mode <25 nm) must appear in the size distribution, and (ii) the new mode must present duration of

10   hours and show growth over time. These requirements were complemented by Ma and Birmili (2015), which described that: (i) sudden increase of PNC in nucleation mode must occur above nocturnal background concentration, (ii) the burst needs to have a minimal of 1 hour, and (iii) a decrease in concentration of the nucleation mode particles is expected at end of day.

Dal Maso et al.(2005) identified two classes of NPF events: (Ia) Clear and strong particle formation event, followed by particle growth; (Ib) When particle growth can be observed from the nucleation, however without a clear nucleation burst;

15   and (II) The particle growth from nucleation mode cannot be determined.

During the day 12, the observed NPF event was in agreement with all the requirements described above. The nucleation burst presented duration of 3h, followed by growth of particles until night, when it was observed a short decrease in the concentration. As discussed earlier, the nucleation events of days 12 and 14 probably presented a great contribution of SOA formation, indicated by local nucleation under higher photochemical activity.

20   The NPF of day 14 was classified as class II, because significant particle growth was not observed after nucleation. This event presented similar nucleation bursts such as observed by Betha et al.(2013) in Singapore and by Cheung et al.(2011) in Brisbane. The authors of their studies associated the events with winds from industrial areas, with large contribution of SO_2 and VOCs.

On days 7, 8 and 10, class Ib events were identified, showing a clear growth of particles along the day. In these days,

25   moderate to high (5–20 µg m^{-3}) SO_2 and NO_x concentrations were observed at the Congonhas CETESB station, which suggest that the initiation of nucleation process occurred near of this station, followed by detection of particles growth at the USP measurement site. Backman et al.(2012) observed similar class Ib events in São Paulo. The NPF events on days 7 and 12 were similar to banana and apple type NPF events, respectively (Wu et al.,2007; Cheung et al., 2011).

In summary, the nucleation of primary aerosol occurs near the sources such as transport and industries emission. Such types

30   of nucleation events were not detected in this study because of the distance between the sources and measurement site. However, 5 different secondary aerosol NPF events were observed; out of which class Ia and II were mostly associated with NO_x and high photochemical activity. While class Ib event were characterized as NPF passing through the measurement site without observation of the initiation of event. The impact of these NPF events in the activated ratio (Fig. 3d) and activation diameter are discussed in Section 3.4.

PND contour plots were drawn in order to evaluate particle nucleation and growth evolution of the different NPF class events and the days without NPF events (Fig. 4). In addition, frequency of hourly PNCs in three modes (nucleation, Aitken and accumulation) and hourly PND were also plotted (Fig. 4). On the day 12, a NPF event with nucleation burst between 1000 and 1500 h was observed (Fig. 4a), which could be confirmed by the highest nucleation percentage of PNC (>50%) in

5   relation with other hours. The particle growth in subsequent hours was accompanied by increase in Aitken mode as can be noted in PNCs hourly frequency and PND hourly graphs (Fig. 4a).

The NPF event (Ib) showed a characteristic particle growth after midday, with probably the occurrence of a nucleation event, not observed between 1000 and 1200 h. This particle evolution was also detected by higher PNC percentage (63%) of Aitken mode at 1500 and the increase of peak diameter between 1200 and 1500 h in hourly PND graph (Fig 4b). Aitken mode

10   predominates for all evaluated hours with values higher than 40% (Fig. 4c). Interestingly, the Aitken mode presented higher percentages (>45%) for most hours on the three selected days, which indicates the continuous increase of new particle events at night. This observation is supported by the local traffic that presents constant emissions, as discuss in Section 3.3, with high density during the day and low density at night, which agrees with total PNC values showed on the top of PNC hourly frequency graphs (Fig.4).

15   **3.3 Apportionment of biomass burning, sea-salt and local sources**

A combination of lidar analysis, Hysplit trajectories and size distributed chemical composition were used to apportion the contribution of sea-salt and biomass burning through the air masses arriving at SPMA. Over the past 30 years, several past studies conducted in SPMA have being using receptor modelling and aerosol chemical composition to identify main sources in its atmosphere (Boueres and Orsini, 1981; Andrade et al., 1994; Castanho and Artaxo, 2001; Sanchez-Ccoyllo& Andrade,

20   2002; Sanchez-Ccoyllo et al., 2008; Andrade et al., 2012). Some studies found BC to be associated mainly with the fossil fuel combustion and biomass burning, while Na and Cl represented sea-salt contribution (Bzdek et al., 2012; Calvo et al., 2013, Taiwo et al. 2014).

Figure 5 shows the mass size distributions of TEC from MOUDI samplers for different periods. Higher concentrations (~0.9%) of BC were observed during the days 6, 12 and 13 (Fig. 5a) compared with intermediate percentages (~0.4 %) on

25   the other days 7, 8, 9 and 14. BC major concentrations for evaluated days occurred in particles lesser than 1 μm. There were no measurements for the day 9 at night (9N).

The elements Cl, K and Pb presented higher values for the days 8 and 9 (Figs. 4b, c and d). Intermediate concentration (0.2 μg cm^{-3}) was observed for K during the day 6. The elements Ti, Fe, Ca and Cu showed intermediate concentrations for most days, with peaks during the day 6 in the morning and day 3 at night for Ti, Ca and Fe, Ca, S, respectively (Figs. 4 e, f, g and

30   h).

The studied elements (Pb, K and Cu) and BC presented higher concentrations in particles smaller than 1 μm, while Ti, Fe, Ca and Cl predominate in particles greater than 1 μm. Normally, natural atmospheric aerosol presents larger particles than anthropogenic ones that contribute to fine (≤2.5 μm) and ultrafine particles (<1μm). This observation is in agreement with

Atmospheric
Chemistry
and Physics
Discussions

Open Access

EGU

the main sources of these elements, in which Ti and Fe are mainly associated with road and soil dust resuspension. However, Fe is also connected with industrial emissions. The sea–salt aerosol is characterized by Cl and Na, while Ca is associated with cement industry represented by construction and demolition activities (Calvo et al., 2013). The K has been used as a marker to biomass burning emissions. However, about 50% of vehicular fuel burned in Brazil is ethanol, derived from

5   sugarcane of vegetation that contains K. Therefore, in this case K is not an efficient marker for biomass burning (Andrade et al.,2012).

As described above, vehicles are the major local air pollution source in SPMA, which is represented by Cu, BC, Zn, Ni and Cr as main inorganic tracer elements for light and duty vehicles (Andrade et al., 2012). The higher concentrations of Cu occurred during days 6 and 13, while other days showed intermediate concentrations, probably associated with constant

10   vehicular traffic. The BC and Cu peaks showed similarity for days 6 and 13.

Previous studies have shown the contribution of sea–salt to the aerosol of SPMA (Andrade et al., 1994; Castanho and Artaxo, 2001; Vara-vela et al., 2015). As can be seen in figure 3b, predominant wind direction was from southeast during the days 7 and 8 at night, which corroborate with air mass trajectories at low altitudes shown in Supplementary Information, SI, figure S1. Hence the higher concentrations of Cl during these days indicate sea–salt transport from the coastal region. This

15   observation is confirmed by increase of Pb concentrations during these days. Normally, Pb element is linked with the emissions from anthropogenic sources, mainly from industrial emissions, as the contribution from fuel burning has decreased substantially after the ban of Pb from gasoline fuels. Gioia et al. (2010) have demonstrated a contribution of Pb from this area to SPMA when southeast wind predominates. There are two large industrial areas southeast of SPMA, one of them on coastal region (Cubatão) (Fig. 1).

20   Elastic backscatter lidar data and air masses modelling trajectories were used to evaluate the relationship of Cl, Pb and BC variability with sea-salt and biomass burning apportionment. The lidar backscatter profiles can provide information about the vertical distribution of aerosol layers, and after associating with air masses trajectories it is possible to infer the source locals and transport time the aerosols plumes arrive to SPMA.

The retrieval of the aerosol optical properties is based on the measurements of the light backscattered by aerosols and thus

25   obtaining the aerosol backscatter coefficient $\beta_{aer}(\lambda, z)$ at 532 nm, from 300 m up to an altitude of 5 to 6 km. The determination of the vertical profile of the aerosol backscatter and extinction coefficients $\alpha_{aer}(\lambda, z)$ relies on the lidar inversion technique following a modified Klett algorithm (Klett, 1981, 1983) under the assumption of the single scattering approximation. To solve the lidar equation requires establishing a relation between $\alpha_{aer}(\lambda, z)$ and $\beta_{aer}(\lambda, z)$. This is typically achieved assuming the aerosol extinction-to-backscatter ratio as independent of altitude; i.e., that $LR(\lambda) =$

30    $\alpha_{aer}(\lambda, z)/\beta_{aer}(\lambda, z)$. However, it is known that the LR depends on several physical-chemical parameters inherent to the aerosols being inspected, such as the aerosol refractive index, and the size and shape distributions of the aerosol particles (Liou, 2002). To derive the appropriate values of the vertical profile of aerosol backscatter coefficient in the lower troposphere, we use an iterative inversion approach that tunes the LR values based on the inter-comparison of the AOD values derived by the lidar and a collocated AERONET sunphotometer (Marenco et al., 2002) or for some cases from values

from MODIS data from AQUA/TERRA satellites (Remer et al., 2005). Once the values of the vertical profile of the aerosol backscatter coefficient are derived (when the difference between the AODs derived by sunphotometer and lidar was less than 10%), we reapply Klett's inversion technique using the appropriate LR values to retrieve the final values of the vertical profiles of the backscatter and extinction coefficient at 532 nm. The vertical profiles of pressure and temperature measured

5   by radio soundings launched twice a day, at 1200 UTC and 0000 UTC, at a distance of about 10 km from the place where the MSP-Lidar system is located, are used to obtain the molecular contribution based in the using Bucholtz's approach (Bucholtz , 1995). The molecular contribution is calculated in an altitude range with negligible particle load, being considered as an aerosol-free region, set here in an altitude range of 8 to 12 km.

Figures 6 c and d present the vertical profile for two measurement days using the MSP-Lidar I system installed about 400 m

10   from the IAG site. On day 6, several thin aerosol plumes above the planetary boundary layer (PBL) were detected. According to the lidar range corrected signal at the right panel of figure 6c, most of aerosol load in atmosphere is concentrated inside the PBL, about 500 meters above the ground level (AGL). However, it can be clearly seen several aerosol layers above the PBL, between 1000 and 2000 m (AGL) and a thin aerosol layer around 3000 m (AGL). The mean aerosol backscatter profile at 532 nm (left panel of figure 6c) retrieved applying the Klett inversion method described

15   previously, show a peak of 0.006 $km^{-1}sr^{-1}$ around 500 m, representing all aerosol trapped inside PBL and another peak of 0.0018 $km^{-1}sr^{-1}$ around 2800 m (AGL). The mean aerosol vertical profile at 532 nm clearly shows a backscatter signal from aerosol plumes up to 4000 m, which should be in general from a source outside SPMA.

When the lidar data analysis is done by tuning the LR values based on the inter-comparison of the MODIS derived AOD, a mean lidar ratio of 70±14 sr is obtained, which is a value associated to absorbing particles from biomass burning (Müller et

20   al., 2007; Baars et al., 2015). The simulated air masses backward trajectories using HYSPLIT model (figure 6a) strengthens the hypothesis that biomass burning aerosol was transported from the North and Central western portion of Brazil, where several focus of fire were found, and then after reaching higher levels are transported to SPMA at altitudes ranging from 3000 to 4000 m (AGL). The same pattern is found when performing an analysis for day 12 (Fig. 6d), when thin aerosol plumes are also detected above the PBL, between 2400 to 4000 m (AGL) as can be seen in the mean backscatter profile

25   (panel left at figure 6d). The mean lidar ratio for this case is also 70±14 sr, again associating the plume to a biomass burning aerosol type. Air masses trajectories in figure 6b indicated that plumes detected at SPMA by the lidar system were transported from the central western portion of Brazil, and traveled across regions with several focus fires. Both lidar analysis and measurements are in agreement with previous analysis of size distribution of elemental concentrations samples collected by MOUDI during the days 6 and 12, when were observed high concentrations of BC. Figure 7c (right panel)

30   shows the range corrected signal of SPMA atmosphere during the whole measured day 4. During the period of 2030 to 2213 (UTC) there were detected a signal attenuation between 500 and 1000 m (AGL), which is associated to the intrusion of clean air at the PBL of SPMA. Usually this clean air intrusion is related to the sea breeze transported to SPMA (Rodrigues et al., 2013). The mean backscatter profile showed the presence of aerosol only within the PBL, where could be seen a smaller

Atmospheric
Chemistry
and Physics
Discussions

aerosol backscatter signal from 300 m up to 1200 m (AGL), associated to the clean air region inside PBL. The mean lidar ratio for this measurement was 40±8 sr, associated to the urban aerosol type (Baars et al., 2015).

3.4 Effect of local and remote sources and NPF events on CCN activation properties

The AR is calculated as a ratio of CCN/PNC, which is described in the literature as "CCN efficiency" or "CCN fraction".
5 This shows the fraction of total particles that are able to produce CCN. The AR value has been extensively published in several papers, which discussed variability of CCN properties over different conditions and pollution events (Table 2). These bulk ratios do not consider aerosol particle size, which is very important to CCN activation. The inorganic salts are present at larger particles (normally >200 nm) and represent most soluble fraction, while organic fraction that is less hydrophilic is found mainly at small particles (<100 nm). Furthermore, Köhler theory predicts that critical supersaturation decrease with
10 the increase in particle size (McFiggans et al., 2006; Andreae and Rosenfield, 2008).

AR average values were 0.22±0.05 (SS 0.2%), 0.33±0.09 (SS 0.4%), 0.41±0.05 (SS 0.6%), 0.48±0.09 (SS 0.8%) and 0.53±0.09 (SS 1.0%). The AR showed a marked difference between nocturnal and diurnal periods; nocturnal average was twice higher than diurnal values for all evaluate SS (tab. 2 and fig. 8a). In addition, PNC was five-times higher for diurnal than nocturnal periods. Figures 3c and 8b show that larger particles predominate at night as result of primary and secondary
15 aerosol growth during the diurnal period. The primary aerosols are mostly emitted during the first rush hour at morning, while secondary aerosol is formed near the noon by nucleation process, as discussed in Section 3.2. Therefore, the higher AR for nocturnal period is expected, according to efficiency of larger particles to act as CCN, associated with lower PNC.

The diurnal period presented average AR values similar to those observed in urban areas, but not at coastal areas, as indicated by recent studies in São Paulo and Vienna (Almeida et al, 2014, Burkart et al., 2012). Additionally, these values are
20 comparable with fresh ship exhaust emission from California City. The nocturnal AR values were similar to those from forest and coastal environments, but frequently lower PNC opposite to those seen in urban environment. Moreover, Aitken and accumulation PNC mode dominates in forest and coastal regions, except during NPF events, as discuss below.

The increase of AR over SS was most pronounced for nocturnal rather than diurnal period as shown in figure 8a. Diurnal period for days with and without the NPF events presented similar slope. Tendencies of lower AR for days with NPF in
25 contrast to days without NPF events could be observed, although with insignificant statistical differences. This observation agrees with previous studies and assumptions that larger particles act most efficiently as CCN than smaller ones (Sihto et al., 2011; Dusek et al., 2010). Some events of NPF bursts, followed by increase of particles, have been observed in Finland (Sihto et al., 2011). During these events, very low AR was observed because of the higher PNC with small size. After the NPF events, was observed substantial increase in the AR.

30 Figure 8b shows the hourly averages of AR for days with and without NPF. The smaller AR values were obtained between 1000 and 1500 h, while the largest values during the night. A decrease in AR started after 0600h and subsequent increase started after 1500 h. In São Paulo city, the first rush hour occurs between 0700 and 1000 h while the second peak from 1700

to 2000 h. The interval of AR decrease and lower values occurred at the same time of first rush hour and formation of secondary aerosol.

The vehicular emission and secondary aerosol formation corresponds to the main source of particles for megacities such as São Paulo. As discussed in Section 3.2, the formation process of secondary aerosol is favoured by photochemical reactions,

5   which depends of solar radiation (in the UV and visible wavelength), ozone and radical species (OH, NO). Figure 3a shows that UV radiation and ozone peaks occur at midday, followed by secondary aerosol formation as demonstrated by intermediate concentrations on nucleation mode after noon (Fig. 3c). Therefore, vehicular emission and secondary aerosol formation probably present the major contribution to fewer AR values along the day.

The increase of AR after 1500 h can be associated with the increase of particles and CCN concentrations. Additionally, the

10   production of SOA by degradation of VOCs can result in formation of polar functional groups that contributes to hydrophilicity of particles. Therefore aged aerosol emitted and formed during the morning from vehicular and secondary particles showed increase of AR at end of afternoon and during night hours. This observation agrees with previous studies, presented in introduction, describing increase of CCN efficiency for aged anthropogenic emissions. On the other hand, vehicular emission from the second rush hour (1700-2000 h) presented lesser effect on AR than the first rush hour, mainly

15   due to the absence of secondary aerosol and mixture with aged aerosol.

The hourly PND clearly shows the effect of particle size on AR values, with lower AR accompanied by smaller particle size modes (Fig. 8b). Our observation agrees with previous studies, presented in introduction, demonstrating strong effect of particle size on CCN activity.

Variability in activation diameter reflects the effect of aerosol chemical composition, associated to hygroscopicity or water

20   activity. Higher numbers of hygroscope particle are activated at small diameter, while hydrophobic particles are usually activated at large diameters (Sihto et al. 2011). Frank et al.(2006) observed activation diameter of 50 nm for pure sulphate and marine aerosol, 70 nm for continental aerosol, represented by regional pollution, and 125 nm for fresh biomass smoke aerosol at SS=0.4% (Andreae and Rosenfield, 2008). Considering a homogeneous chemical composition of the particles, apparent activation diameter ($D_{act,a}$) can be calculated by integration of size distributed aerosol from larger particles towards

25   smaller ones until the integral equals CCN concentration at a given SS (Bulkart et al., 2011). However, the atmospheric aerosol presents a variable and complex composition over size distribution, containing different percentages of soluble and insoluble compounds. Therefore this consideration must be taken into account to adequately discussion.

The average $D_{act,a}$ varied between 54 (SS 1.0%) and 155 nm (SS 0.2%) for nocturnal and diurnal periods, respectively. Comparison of average $D_{act,a}$ with the literature are shown in SI Table S1. As can be seen in figure 9a, $D_{act,a}$ presents non-

30   linear decrease as function of increase in SS. Diurnal period showed highest $D_{act,a}$ opposite to nocturnal ones, as expected according earlier AR discussion. Average $D_{act,a}$ for hours during sea-salt apportionment for nocturnal period presented the lowest values, while average $D_{act,a}$ during biomass burning for nocturnal period had similar values that total nocturnal average. However for SS <0.4%, biomass burning showed values slightly higher than nocturnal average. Other works have reported that $D_{act,a}$ increase significantly for lower SS than for higher SS, due to the increase of solute effect. Weak impact on

CCN activity is observed at high SS for particles with different chemical composition and therefore hygroscopicity (Sihto et al., 2011; Zhang et al., 2014).

Figure 9b shows the time series of average $D_{act,a}$ for days with and without NPF events. As expected, NPF days presented higher activation diameters in relation to days without NPF during rush hour. Additionally, lower AR (Fig. 8b) and higher

5   $D_{act,a}$ (Fig. 9b) were observed during NPF days at some hours before event occurrence, where lower PNC and larger particles (Fig.3c and Fig.9b) predominated. This observation can be related to possibly increase in fresh SOA and precursor compounds at gas and condensed phases before NPF event. Some of these substances must be represented by monoterpenes and aromatic compounds, which present low hygroscopicity (Kroll and Seinfeld, 2008). For example, Prenni et al. (2007) demonstrated the moderately hygroscopicity ($k\sim0.1$) of fresh SOA produced from toluene and terpene precursor in a smog

10   chamber. Moreover, authors showed by model calculation that CCN activity for the mixture between fresh SOA and sulphates were similar to insoluble organic particles. Apart from these previous NPF hours, days with and without NPF event showed similar nocturnal averages.

AR and $D_{act,a}$ are useful parameters to represent CCN activity of aerosols, in which AR variability is associated with size and chemical composition of aerosol while $D_{act,a}$ is related with chemical composition only (Furutani et al., 2008). AR versus

15   $D_{act,a}$ for SS=0.4% showed a non-linear correlation that can indicate different chemical and size combination of aerosol during diurnal and nocturnal periods (Fig. 9c). These periods were fitted separately and presented linear anti-correlation between AR and $D_{act,a}$. The diurnal period showed higher $D_{act,a}$ and lower AR values associated with smaller and less hygroscopic particles. On the other hand, nocturnal presented opposite behaviour, with large size and high hygroscopic aerosol. Additionally, diurnal pattern is related mainly with fresh traffic emission while nocturnal with aged aerosol and sea

20   salt air masses. It can be observed that nocturnal samples are most related with water soluble species as $(NH_4)_2SO_4$, SOA, NO_3^- and marine air than the diurnal aerosol. Our observations agree with prior studies that showed high hygroscopicity for aged aerosol, which are similar to marine air masses (fig. 10).

Figure 10 shows comparison of $D_{act,a}$ obtained in this and published studies. The nocturnal values are similar with those from Shangai for continental air masses, Finland for boreal forest and California for periods without air masses of anthropogenic

25   emissions. Diurnal values are near of that urban/industrial from California and Mexico, and fresh ship exhaust.

The $D_{act,a}$ for periods during the biomass burning and sea salt plumes from remote regions showed no difference in diurnal averages (data not showed). However, some tendencies could be noted for nocturnal periods, even with insignificant statistical differences. $D_{act,a}$ average for period with sea-salt events present values near to those observed for Atlantic and Pacific Oceans, Gulf of Mexico, without direct anthropogenic air masses, and aged anthropogenic emission from California.

30   It must be taken into account that nocturnal aged aerosol of anthropogenic sources are presented for all days, therefore lower $D_{act,a}$ were observed during sea salt events, due to additional contribution from this source. Nocturnal average values were found to be comparable with urban/industrial and fresh polluted air masses from Mexico and California cities, as shown in figure 10.

4 Summary and conclusions

The CCN activation is very important to cloud formation and consequently to hydrological cycle. The aim of this study was to study the CCN activation parameters variability under air masses from local and remote sources and during NPF in order to assess the impact of these events on CCN activity for the São Paulo Metropolitan Area (SPMA). The region is highly

5   impacted by the local emission of mobile sources and by the transport of biomass burning, industrial and sea-salt particles.

The diurnal period presented higher PNC and smaller particle sizes than nocturnal ones, associated with traffic fresh emissions and NPF, while lower PNC values and large particles size were observed at night due to aging and deposition of particles after growth (Fig. 11a). Five NPF events were identified, being four of class I type. Moreover, NPF events showed significant effect on particle size distribution. Biomass burning and sea-salt air masses were identified by combination of

10   lidar analysis, Hysplit trajectories and chemical composition size distribution.

The AR and $D_{act,a}$ CCN activation parameters presented a clear pattern for diurnal and nocturnal periods, in which diurnal period was marked by higher $D_{act,a}$ and lower AR, while nocturnal showed opposite behaviour. The size distribution had visible contribution for this pattern, according to the assumption that larger particles are more efficient for CCN activation than smaller ones. This hypothesis is verified by AR and $D_{act,a}$ differences for days with and without NPF events. Slight

15   differences for activation parameters could be observed between ea salt and biomass burning air masses and nocturnal average (Fig. 11b,c). These little differences can be explained by complex mixtures between aerosol from local and external sources, where the second travel longer distances before reaching to measurement site. Dilution, mixing and aging of aerosol from remote sources can occur during travel from source emission area and measurement site. $D_{act,a}$ calculated for sea-salt air masses in this study were comparable with activation diameter from Atlantic and Pacific Oceans. In summary, local traffic

20   emissions showed higher influence on activation parameters than remote sources.

This was the first study for the SPMA to evaluate effects of remote sources and NPF events on CCN activation properties, and the second to assess CCN variability in this area. Our results showed the influence of local emissions, long-range transport of sea salt and biomass burning plumes, and NPF on CCN properties. Therefore, long-term studies covering different seasons and sampling site environments (e.g. coastal, urban and rural) are needed to better represent CCN

25   variability over diverse environmental conditions. In order to better understand the influence of aerosol composition and provenience on CCN activity, real-time monitoring of aerosol chemical composition and CCN size distributed is also essential.

5 Acknowledgements

Atmospheric
Chemistry
and Physics
Discussions

Open Access

EGU

5 **References**

Almeida, G.P., Brito, J., Morales, C.A., Andrade, M.F., Artaxo, P.: Measured and modelled Cloud Condensation Nuclei (CCN) concentration in São Paulo , Brazil: the importance of aerosol size-resolved chemical composition on CCN concentration prediction, Atmos. Chem. Phys., 13, 1–36, 2014.

10 An, J., Wang, H., Shen, L., Zhu, B., Zou, J., Gao, J., & Kang, H.: Characteristics of new particle formation events in Nanjing, China: Effect of water-soluble ions, Atmos. Environ., 108, 32–40,2015.

Andrade, M.F., De Miranda, R. M., Fornaro, A., Kerr, A., Oyama, B., De Andre, P. A., Saldiva, P.: Vehicle emissions and PM 2.5 mass concentrations in six Brazilian cities, Air Qual., Atmos. Health, 5, 79–88, 2012.

Andrade, M.F., Orsini, C., Maenhaut, W.: Relation between aerosol sources and meteorological parameters for inhalable atmospheric particles in Sao Paulo City, Brazil, Atmos. Environ., 28, 2307–2315, 1994.

15 Andreae, M. O., Rosenfeld, D., Artaxo, P., Costa, a a, Frank, G. P., Longo, K. M., Silva-Dias, M. A. F.: Smoking rain clouds over the Amazon, Science, 303, 1337–1342, 2004.

Andreae, M. O., Rosenfeld, D.: Aerosol–cloud–precipitation interactions. Part 1. The nature and sources of cloud-active aerosols, Earth-Sci. Rev., 89, 13–41, 2008.

Baars, H., Kanitz, T., Engelmann, R., Althausen, D., Heese, B., Komppula, M., Preißler, J., Tesche, M., Ansmann, A.,

20 Wandinger, U., Lim, J.-H., Ahn, J. Y., Stachlewska, I. S., Amiridis, V., Marinou, E., Seifert, P., Hofer, J., Skupin, A., Schneider, F., Bohlmann, S., Foth, A., Bley, S., Pfüller, A., Giannakaki, E., Lihavainen, H., Viisanen, Y., Hooda, R. K., Pereira, S., Bortoli, D., Wagner, F., Mattis, I., Janicka, L., Markowicz, K. M., Achtert, P., Artaxo, P., Pauliquevis, T., Souza, R. A. F., Sharma, V. P., van Zyl, P. G., Beukes, J. P., Sun, J. Y., Rohwer, E. G., Deng, R., Mamouri, R. E., Zamorano, F. PollyNET: a global network of automated Raman-polarization lidars for continuous aerosol profiling. Atmos. Chem. Phys.

25 Discuss., 15, 27943 – 28004, Doi: 10.5194/acpd-15-27943-2015, 2015.

Backman, J., Rizzo, L. V., Hakala, J., Nieminen, T., Manninen, H. E., Morais, F., Kulmala, M.: On the diurnal cycle of urban aerosols, black carbon and the occurrence of new particle formation events in springtime São Paulo, Brazil,Atmos. Chem. Phys., 12, 11733–11751, 2012.

Baumgardner, D.: Evidence for the formation of CCN by photochemical processes in Mexico City, Atmos. Environ., 38,

30 357–367, 2004.

Betha, R., Spracklen, D. V., Balasubramanian, R.: Observations of new aerosol particle formation in a tropical urban atmosphere, Atmos. Environ., 71, 340–351. 2013.

17

Atmospheric
Chemistry
and Physics
Discussions

Bouéres, L.C.S., Orsini, C.M.Q.: Fine and coarse elemental components in the urban aerosol of São Paulo, Brazil,NuclInstrum Methods, 181:417–424, 1981.

Bougiatioti, A., Nenes, A., Fountoukis, C., Kalivitis, N., Pandis, S. N., & Mihalopoulos, N.: Size-resolved CCN distributions and activation kinetics of aged continental and marine aerosol. Atmos. Chem. Phys., 11, 8791–8808, 2011.

5 Bucholtz, A.: Rayleigh-scattering calculations for the terrestrial atmosphere, Appl. Optics, 34, 2765-2773, doi:10.1364/AO.34.002765, 1995.

Burkart, J., Steiner, G., Reischl, G., Hitzenberger. R.: Long-term study of cloud condensation nuclei (CCN) activation of the atmospheric aerosol in Vienna, Atmos. Environ., 45, 5751-5759, 2011.

Bzdek, B. R., Pennington, M. R., Johnston, M. V.: Single particle chemical analysis of ambient ultrafine aerosol: A review,

10 J. Aerosol Sci., 52, 109–120, 2012.

Calvo, a. I., Alves, C., Castro, a., Pont, V., Vicente, a. M., Fraile, R.: Research on aerosol sources and chemical composition: Past, current and emerging issues, Atmos. Res., 120-121, 1–28, 2013.

Castanho, D. A., Artaxo, P.: Wintertime and summertime São Paulo aerosol source apportionment study, Atmos. Environ., 35, 4889–4902, 2001.

15 Cheung, H. C., Morawska, L., Ristovski, Z. D.: Observation of new particle formation in subtropical urban environment, Atmos. Chem. Phys., 11, 3823–3833, 2011.

Dal Maso, M., Kulmala, M., Riipinen, I., Wagner, R., Hussein, T., Aalto, P. P., &Lehtinen, K. E. J. Formation and growth of fresh atmospheric aerosols: eight years of aerosol size distribution data from SMEAR II, Hyytiala, Finland, Boreal Environ. Res., 10, 323–336, 2005.

20 Deng, Z. Z., Zhao, C. S., Ma, N., Ran, L., Zhou, G. Q., Lu, D. R., & Zhou, X. J.:An examination of parameterizations for the CCN number concentration based on in situ measurements of aerosol activation properties in the North China Plain,Atmos. Chem. Phys., 13, 6227–6237,2013.

Draxler, R., and G. Hess (1998), Description of the hysplit 4 modeling system, NOAA Tech. Memo. ERL ARL-224, NOAA Air Resources Laboratory, Silver Spring, MD, USA, [Available Online at http://ready.arl.noaa.gov/HYSPLIT.php].

25 Dusek, U., Frank, G. P., Curtius, J., Drewnick, F., Schneider, J., Kürten, A., Pöschl, U.: Enhanced organic mass fraction and decreased hygroscopicity of cloud condensation nuclei (CCN) during new particle formation events. Geophys. Res. Lett., 37, 2010.

Frank, G.P., Dusek, U., Andreae, M.O.: A method for measuring size-resolved CCN in the atmosphere, Atmos. Chem. Phys. Discuss., 6, 4879–4895, 2006.

30 Freud, E., Rosenfeld, D., Andreae, M. O., Costa, A. A., Artaxo, P.: Robust relations between CCN and the vertical evolution of cloud drop size distribution in deep convective clouds, Atmos. Chem. Phys., 8, 1661–1675, 2008.

Furutani, H., Dall, M., Roberts, G. C., Prather, K. A.: Assessment of the relative importance of atmospheric aging on CCN activity derived from field observations, Atmos. Environ., 42, 3130–3142, 2008.

Atmospheric
Chemistry
and Physics
Discussions

Gioia, S.M.C.L., Babinski, M., Weiss, D.J., Kerr, A.A.F.S.: Insights into the dynamics and sources of atmospheric lead and particulate matter in São Paulo, Brazil, from high temporal resolution sampling, Atmos. Res., 98,478–485, 2010.

Guerrero-Rascado, J. L., Landulfo, E., Antuña, J. C., Barbosa, H. M. J., Barja, B, Bastidas, A. E., Bedoya, A. E., da Costa, R. F., Estevan, R., Forno, R. N., Gouveia, D. A., Jimenez, C., Larroza, E. G., Lopes, F. J. S., Montilla-Rosero, E., Moreira,

5   G. A., Nakaema, W. M., Nisperuza, D., Alegria, D., Múnera, M., Otero, L., Papandrea, S., Pawelko, E., Quel, E. J., Ristori, P., Rodrigues, P. F., Salvador, J., Sánchez, M. F., Silva, A. Towards an instrumental harmonization in the framework of LALINET: dataset of technical specifications in Proc. SPIE 9246, Lidar Technologies, Techniques, and Measurements for Atmospheric Remote Sensing X, 92460O, doi: 10.1117/12.2066873, 2014.

Guerrero-Rascado, J. L., Landulfo, E., Antuña, J. C., Barbosa, H. M. J., Barja, B, Bastidas, A. E., Bedoya, A. E., da Costa,

10   R. F., Estevan, R., Forno, R. N., Gouveia, D. A., Jimenez, C., Larroza, E. G., Lopes, F. J. S., Montilla-Rosero, E., Moreira, G. A., Nakaema, W. M., Nisperuza, D., Alegria, D., Múnera, M., Otero, L., Papandrea, S., Pawelko, E., Quel, E. J., Ristori, P., Rodrigues, P. F., Salvador, J., Sánchez, M. F., Silva, A. Latin American Lidar Network (LALINET) for aerosolresearch: Diagnosison network instrumentation. J Atmos Sol-TerrPhy, 138-139, 112-120, 2016.

Guerrero-Rascado, L., Landulfo, E., Antuña, J. C., Barbosa, H. M. J., Barja, B.. Bastidas, A.E., Bedoya, A.E., Da Costa, R.

15   F.,Estevan, R., Forno, R., Gouveia, D.A., Jimnez, C., Larroza, E.G., Lopes, F. J. S.,Montilla-Rosero, E., Moreira, G. A.,Nakaema, W. M.,Nisperuza, D., Otero, L.,Papandrea, S., Pawelko, E., Quel, E. J., Ristori, P., Rodrigues, P. F., Salvador, J., Sánchez, M. F., Silva, A.:"Towardsaninstrumentalharmonization in the framework of LALINET: datasetoftechnicalspecifications" in Proc. SPIE 9246, Lidar Technologies, Techniques, and Measurements for Atmospheric Remote Sensing, 92460O, 2014.

20   Heal, M.R., Kumar, P., Harrison, R.M. Particles, Air Quality, Policy and Health. Chem. Soc. Reviews 41, 6606-6630, 2012.

Holmes, N. S.: A review of particle formation events and growth in the atmosphere in the various environments and discussion of mechanistic implications, Atmos. Environ., 41, 2183–2201, 2007.

IBGE – Instituto Brasileiro de Geografia e Estatística (http://www. ibge.gov.br/english/) <http://www.ibge.gov.br/home/estatistica/populacao/estimativa2014/estimativa_dou.shtm>Accessed01January 2016.

25   IPCC: Climate change 2013: Scientific basis, Fifth assessment ofthe Inter-governmental Panel on Climate Change, Cambridge, Univ. Press, New York, 2013.

Klett, J. D.: Stable analytical inversion solution for processing lidar returns, Appl. Optics, 20, 211, 1981.

Klett, J. D.: Lidar calibration and extinction coefficients, Appl. Optics, 22, 514, 1983.

Kroll, J. H., & Seinfeld, J. H.: Chemistry of secondary organic aerosol: Formation and evolution of low-volatility organics in

30   the atmosphere, Atmos. Environ., 42, 3593–3624, 2008.

Kulmala, M., Laaksonen, A.: Binary nucleation of water–sulphuric acid system: comparison of classical theories with different H_2SO_4 saturation vapor pressures, J. Chem. Phys. 93, 696, 1990.

Kulmala, M., Vehkamaki, H., Petäjä, T., Dal Maso, M., Lauri, A., Kerminen, V.M., Birmili, W., McMurry, P. H.: Formation and growth rates of ultrafine atmospheric particles: a review of observations, J. Aerosol Sci., 35, 143–176, 2004.

Kumar, P., Robins, A., Vardoulakis, S., Britter, R.: A review of the characteristics of nanoparticles in the urban atmosphere and the prospects for developing regulatory control. Atmos. Environ., 44, 5035-5052, 2010.

Kumar, P., Ketzel, M., Vardoulakis, S., Pirjola, L., Britter, R.: Dynamics and dispersion modelling of nanoparticles from road traffic in the urban atmospheric environment - a review. J. Aerosol Sci., 42, 580-603, 2011.

5 Kumar, P., Morawska, L., Birmili, W., Paasonen, P., Hu, M., Kulmala, M., Harrison, R.M., Norford, L., Britter, R.: Ultrafine particles in cities. Environ. Int., 66, 1-10, 2014.

Leng, C., Cheng, T., Chen, J., Zhang, R., Tao, J., Huang, G., Li, L.: Measurements of surface cloud condensation nuclei and aerosol activity in downtown Shanghai, Atmos. Environ., 69, 354–361, 2013.

Lim, Y.B., Ziemann, P.J.: Products and mechanism of secondary organic aerosol formation from reactions of n- alkanes with

10 OH radicals in the presence of NOx, Environ. Sci. Technol., 39, 9229–9236, 2005.

Liou, K. N. (Ed.) (2002), An Introduction to Atmospheric Radiation, 2nd ed., 583 pp., Academic Press, California.

Ma, N.,Birmili, W.: Estimating the contribution of photochemical particle formation to ultrafine particle number averages in an urban atmosphere, Sci. Total Environ., 512-513, 2015.

Marenco, F., V. Santacesaria, A. F. Bais, D. Balis, A. di Sarra, A. Papayannis, and C. Zerefos.: Optical properties of

15 tropospheric aerosols determined by lidar and spectrophotometric measurements (Photochemical Activity and Solar Ultraviolet Radiation campaign), Appl. Optics, 36, 6875-6886, doi:10.1364/AO.36.006875, 2002.

Mcfiggans, G., Artaxo, P., Baltensperger, U., Coe, H., Facchini, M. C., Feingold, G., Paulo, C. E. P. S. (2006). The effect of physical and chemical aerosol properties on warm cloud droplet activation, Atmos. Chem. Phys., 6, 2593–2649, 2006.

Merikanto, J., Nepari, I., Vehkamaki, H., Anttila, T., Kulmala, M.: New parameterization of sulfuric acid-ammonia-water

20 ternary nucleation rates at tropospheric conditions, J. Geophys. Res., 112, D15207, 2007.

Müller, D., Ansmann, A., Mattis, I., Tesche, M., Wandinger, U., Althausen, D., Pisani, G.: Aerosol-type-dependent lidar ratios observed with ramanlidar. Journal of Geophysical Reasearch 112, D16202, 2007.

Nepari, I., Noppel, M., Vehkamaki, H., Kulmala, M.: Parameterization of ternary nucleation rates for H_20-H_2SO_4-NH_3 vapors, J. Geophys. Res., 112, D15207, 2002.

25 Ng, N.L., Kroll, J.H., Chan, A.W.H., Chhabra, P.S., Flagan, R.C., Seinfeld, J.H.: Secondary organic aerosol formation from m-xylene, toluene, and benzene,Atmos.Chem.Phy., 7, 3909–3922, 2007.

Nie, W., Ding, A., Wang, T., Kerminen, V.-M., George, C., Xue, L., Kulmala, M.: Polluted dust promotes new particle formation and growth, Scientific Reports, 4, 6634, 2014.

Papayannis, A., and G. Chourdakis, The EOLE Project: A multiwavelength laser remote sensing (lidar) system for ozone and

30 aerosol measurements in the troposphere and the lower stratosphere. Part II: Aerosol measurements over Athens, Greece, International Journal of remote Sensing, 23, 179-196, doi:10.1080/01431160010025952, 2002.

Paramonov, M., Aalto, P. P., Asmi, a., Prisle, N., Kerminen, V. M., Kulmala, M., &Petäjä, T.: The analysis of size-segregated cloud condensation nuclei counter (CCNC) data and its implications for cloud droplet activation. Atmos. Chem. Phys., 13, 10285–10301, 2013.

Peng, J. F., Hu, M., Wang, Z. B., Huang, X. F., Kumar, P., Wu, Z. J., He, L. Y.: Submicron aerosols at thirteen diversified sites in China: size distribution, new particle formation and corresponding contribution to cloud condensation nuclei production, Atmos. Chem. Phys., 14, 10249–10265, 2014.

Quinn, P. K., Bates, T. S., Coffman, D. J., & Covert, D. S.: Influence of particle size and chemistry on the cloud nucleating properties of aerosols. Atmos. Chem. Phys., 7, 14171–14208, 2008.

Reade, L., Jennings, S. G.,McSweeney, G.: Cloud condensation nuclei measurements at Mace Head, Ireland, over the period 1994–2002, Atmos. Res., 82, 610–621, 2006.

Remer, L. A., Kaufman, Y. J., Tanré, D., Mattoo, S., Chu, D. A., Martins, J. V., Li, R. R., Ichoku, C., Levy, R. C., Kleidman, R. G., Eck, T. F., Vermote, E., and Holben, B. N.: The MODIS aerosol algorithm, products, and validation, J. Atmos. Sci., 62, 947–973, doi:10.1175/JAS3385.1, 2005.

Roberts, G. C., Nenes, A.: A Continuous-Flow Streamwise Thermal-Gradient CCN Chamber for Atmospheric Measurements, Aerosol Sci. Technol., 39, 206–221. 2005.

Rodrigues, P.F., Landulfo, E., Gandu, A. W., Lopes, F.J.S., Assessment of aerosol hygroscopic growth using an elastic LIDAR and BRAMS simulation in urban metropolitan areas, AIP Conf. Proc. 1531, 360, 2013; doi: 10.1063/1.4804781

Seinfeld J.H. &Pandis S.N.: Atmospheric chemistry and physics: from air pollution to climate change, John Wiley and Sons, New York, 2006.

Sihto, S.L., Mikkilä, J., Vanhanen, J., Ehn, M., Liao, L., Lehtipalo, K., Kulmala, M.: Seasonal variation of CCN concentrations and aerosol activation properties in boreal forest. Atmos. Chem. Phys., 11, 13269–13285, 2011.

Sorribas, M., Adame, J. a, Olmo, F. J., Vilaplana, J. M., Gil-Ojeda, M., &Alados-Arboledas, L.: A long-term study of new particle formation in a coastal environment: meteorology, gas phase and solar radiation implications. Sci. Total Environ., 511, 723–37, 2014.

Taiwo, A. M., Harrison, R. M., & Shi, Z.: A review of receptor modelling of industrially emitted particulate matter, Atmospheric Environment, 97, 109–120, 2014.

Vara-Vela, A, Andrade, M. F., Kumar, P., Ynoue, R. Y., Muñoz, A. G.: Impact of vehicular emissions on the formation of fine particles in the Sao Paulo Metropolitan Area: a numerical study with the WRF-Chem model, Atmos. Chem. Phys., 16, 777-797, 2016.

Wu, Z., Hu, M., Liu, S., Wehner, B., Bauer, S., Wiedensohler, A., Petäjä, T., DalMaso, M., Kulmala, M.:Newparticle formation in Beijing, China: statistical analysis of a 1-year data set, J. Geophys. Res., 112,D09209, 2007.

Yue, D. L., Hu, M., Zhang, R. Y., Wu, Z. J., Su, H., Wang, Z. B., Wiedensohler, A.: Potential contribution of new particle formation to cloud condensation nuclei in Beijing, Atmos. Environ., 45, 6070–6077, 2011.

Yum, S.S., James, G.H., Keun, Y.S., Byoung-Cheol, C.: Springtime cloud condensation nuclei concentrations on the west coast of Korea, Geophys. Res. Lett., 32, L09814, 2005.

Zhang, F., Li, Y., Li1, Z., Sun, L., Li, R., Zhao, R., Wang, P., Sun, Y., Liu, X., Li, J., Li, P., Ren, G., Fan, T. Aerosol hygroscopicity and cloud condensation nuclei activity during the AC3Exp campaign: implications for cloud condensation nuclei parameterization. Atmos. Chem. Phys., 14, 13423–13437, 2014.

Zhang, R., Suh, I., Zhao, J., Zhang, D., Fortner, E.C., Tie, X., Molina, L.T., Molina, M.J.: Atmospheric new particle
5 formation enhanced by organic acids, Science, 304, 1487-1490, 2004.

Zhang, R.,Wang, L., Khalizov, A.F., Zhao, J., Zheng, J., McGraw, R.L., Molina, L.T.: Formation of nanoparticles of blue haze enhanced by anthropogenic pollution, Proc. Natl. Acad. Sci. U. S. A, 106, 17650-17654, 2009.

10

15

20

25

30

Atmospheric
Chemistry
and Physics
Discussions

Table 1. Diurnal data of meteorological (Temperature, Relative Humidity and Rain), PNC and CCN during evaluated period (August, 19 to September, 03). Note that PNC±SD and CCNC±SD are represented by mean value ± standard deviation. Peak diameter was calculated by mode of size distribution.

Day		Date	Meteorological Parameters		Rain	Mean PNC ± SD	PNC (min-max)	Peak Diameter	Mean CCNC ± SD				
			Temperature (°C) mean (min-max)	RH (%) mean (min-max)	(mm)	cm^{-3}	cm^{-3}	Dp (nm)	0.20%	0.40%	0.60%	0.80%	1.0%
1	Tue	8/19/14	15 (11 - 20)	83 (64 - 96)	0.0	7654 ± 4582	1874 - 16607	50	1688 ± 569	1809 ± 624	2270 ± 830	2555 ± 965	2811 ± 1029
2	Wed	8/20/14	16 (11 - 23)	80 (43 - 98)	0.0	13086 ± 8242	3335 - 35398	45	2240 ± 780	2385 ± 961	2969 ± 1191	3431 ± 1371	3770 ± 1611
3	Thu	8/21/14	18 (13 - 27)	70 (32 - 95)	0.0	14133 ± 7647	3360 - 27144	54	2683 ± 1019	3082 ± 1451	3726 ± 1715	4201 ± 1831	4562 ± 1933
4	Fri	8/22/14	19 (12 - 28)	62 (30 - 92)	0.0	15921 ± 7935	5529 - 35508	73	3368 ± 2664	2487 ± 1034	3208 ± 1512	3699 ± 1766	3960 ± 1890
5	Sat	8/23/14	20 (13 - 28)	58 (28 - 87)	0.0	15923 ± 7644	5595 - 32061	72	3889 ± 752	4708 ± 1309	5633 ± 1588	6296 ± 1800	6860 ± 1894
6	Tue	8/26/14	19 (16 - 23)	76 (48 - 96)	1.3	13091 ± 4965	5758 - 26105	92	2765 ± 411	5135 ± 1908	5961 ± 2242	6343 ± 2336	6678 ± 2522
7	Wed	8/27/14	15 (10 - 20)	79 (55 - 93)	0.1	8627 ± 4965	1924 - 20416	50	1103 ± 549	1444 ± 954	1822 ± 1304	2229 ± 1405	2507 ± 1592
8	Thu	8/28/14	13 (10 - 18)	84 (62 - 96)	0.0	11313 ± 6449	4920 - 25556	42	1432 ± 438	2103 ± 1181	2672 ± 1388	3117 ± 1536	3538 ± 1702
9	Fri	8/29/14	13 (12 - 16)	85 (74 - 91)	0.0	9873 ± 3751	5170 - 17513	37	1609 ± 275	2201 ± 529	2747 ± 723	3146 ± 823	3444 ± 861
10	Sat	8/30/14	16 (12 - 22)	80 (48 - 94)	0.0	12601 ± 8315	4486 - 30528	53	1945 ± 384	3144 ± 1142	3856 ± 1380	4304 ± 1632	4734 ± 1743
11	Sun	8/31/14	18 (14 - 30)	83 (30 - 96)	2.2	7078 ± 4543	2781 - 18794	63	1573 ± 679	2144 ± 998	2525 ± 1159	2800 ± 1277	3036 ± 1366
12	Mon	9/1/14	19 (15 - 26)	75 (48 - 95)	0.1	11014 ± 8580	2196 - 31674	38	782 ± 661	1315 ± 1011	1959 ± 1273	2336 ± 1263	2757 ± 1510
13	Tue	9/2/14	19 (14 - 27)	79 (46 - 96)	3.6	14842 ± 10075	2294 - 32152	67	2138 ± 661	3861 ± 1564	4718 ± 1922	5281 ± 2073	5757 ± 2135
14	Wed	9/3/14	18 (15 - 25)	80 (57 - 96)	2.2	7713 ± 7303	1347 - 26928	29	609 ± 328	727 ± 428	981 ± 580	1237 ± 701	1523 ± 834
Mean	-	-	17 (10 - 30)	79 (28 - 98)	0.9	11634 ± 3077	1347 - 35508	55	1987 ± 942	2610 ± 1264	3218 ± 1435	3641 ± 1512	3996 ± 1572

5

10

15

20

25

Atmospheric
Chemistry
and Physics
Discussions

5

Table 2. Activated ratio average (CCN/CN) and particle number concentration (PNC) observed in this study and comparison with data
from literature for different SS and environment.

Reference		Site	Environment	0.20%	0.40%	0.60%	0.80%	1.0%	PNC (x10⁴) cm⁻³
This study	Total mean	Sao Paulo	Urban	0.19±0.12	0.24±0.16	0.30±0.19	0.35±0.20	0.38±0.22	1.2±0.77
	Diurnal	Sao Paulo	Urban	0.13±0.08	0.16±0.09	0.19±0.10	0.22±0.11	0.52±0.21	1.6±0.78
	Nocturnal			0.24±0.12	0.33±0.15	0.41±0.18	0.47±0.19	0.24±0.12	0.3±0.69
Almeida et al.(2014)		Sao Paulo	Urban	0.10±0.05	0.19±0.09	0.23±0.10	0.26±0.11	0.28±0.12	1.3±0.54
Andreae et al.(2004)		Amazon	Forest	-	-	-	-	0.68[a]	0.05[a]
Leng et al.(2013)		Shangai	Urban/Coast	-	-	-	0.4[b] and 0.6[c]	-	0.5[b] - 1.0[c]
Burkart et al.(2011)		Vienna	Urban	-	0.13[d]	-	-	-	0.9 - 5.4
Sihto et al.(2011)		Finland	Forest	-	0.21 - 0.42	-	-	-	~0.2
Yum et al.(2005)		Korea	Urban/Coast	-	-	-	-	0.43[c] - 0.74[b]	0.4[c] - 0.8[b]
Furutani et al.(2008)		California	Urban/Coast	-	-	0.4 - 0.6[e]	-	-	0.2 - 1.5[e]
				-	-	0.06 - 0.2[f]	-	-	1.5 - 3.0[f]
		Pacific Ocean	Over Ocean	-	-	0.6 - 1.0	-	-	0.2 - 0.6

a - Green ocean   d - SS = 0.5%
b - Continental air   e - Anthropogenic polluted air masses
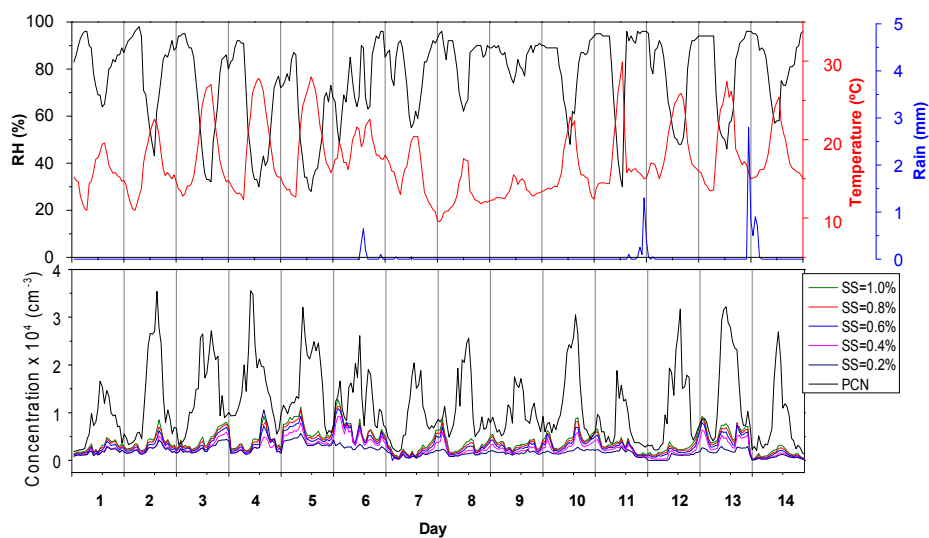c - Marine air   f - Fresh Ship Exhaust

15

20

24

5
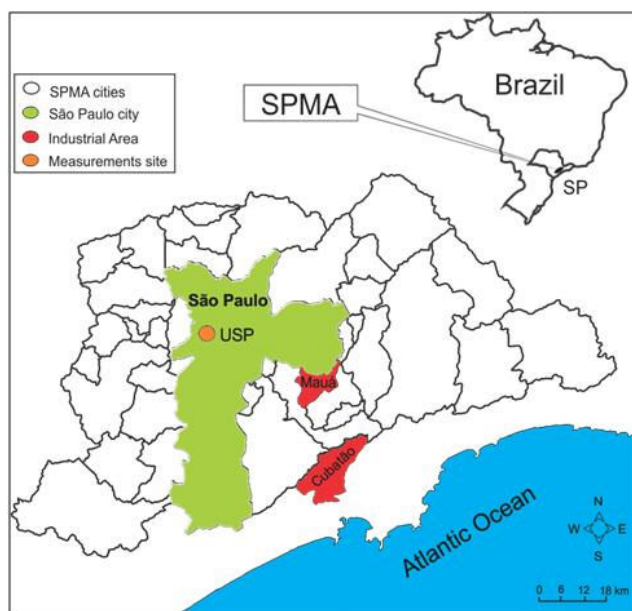
10

Figure 1. Map of São Paulo Metropolitan Area (SPMA). São Paulo city is represented by green colour. Measurements and sampling sites are located inside the University of São Paulo, represented by orange circle. Cubatão and Mauá cities that contain large industrial areas are marked by red colour.
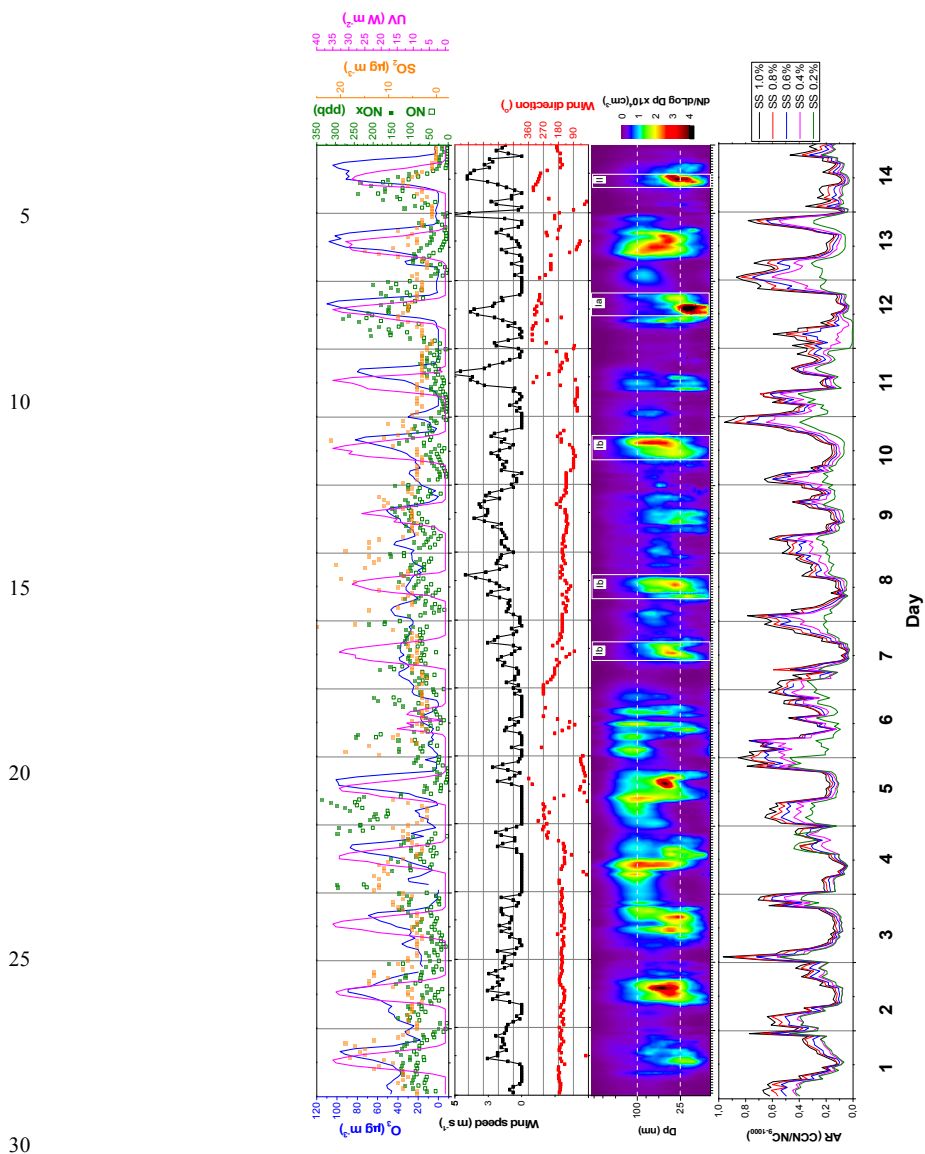
5

10

Figure 2. Meteorological parameters, PNC and CCN hourly variability for the studied period. Note that PNC correspond to size distribution of 9–1000 nm, while CCN of 10 – 2500 nm.

15

Atmospheric
Chemistry
and Physics

Open Access

Discussions

EGU

Figure 3. Hourly variability of a) UV radiation, SO$_2$, NO$_x$, NO$_2$ and O$_3$ concentrations, b) wind direction and speed, c) PND and d) Activated Ratio (CCN/CN). UV radiation, SO$_2$, O$_3$, NO$_x$ and NO$_2$ concentrations was provided by CETESB.

Atmospheric
Chemistry
and Physics
Discussions
Open Access
EGU
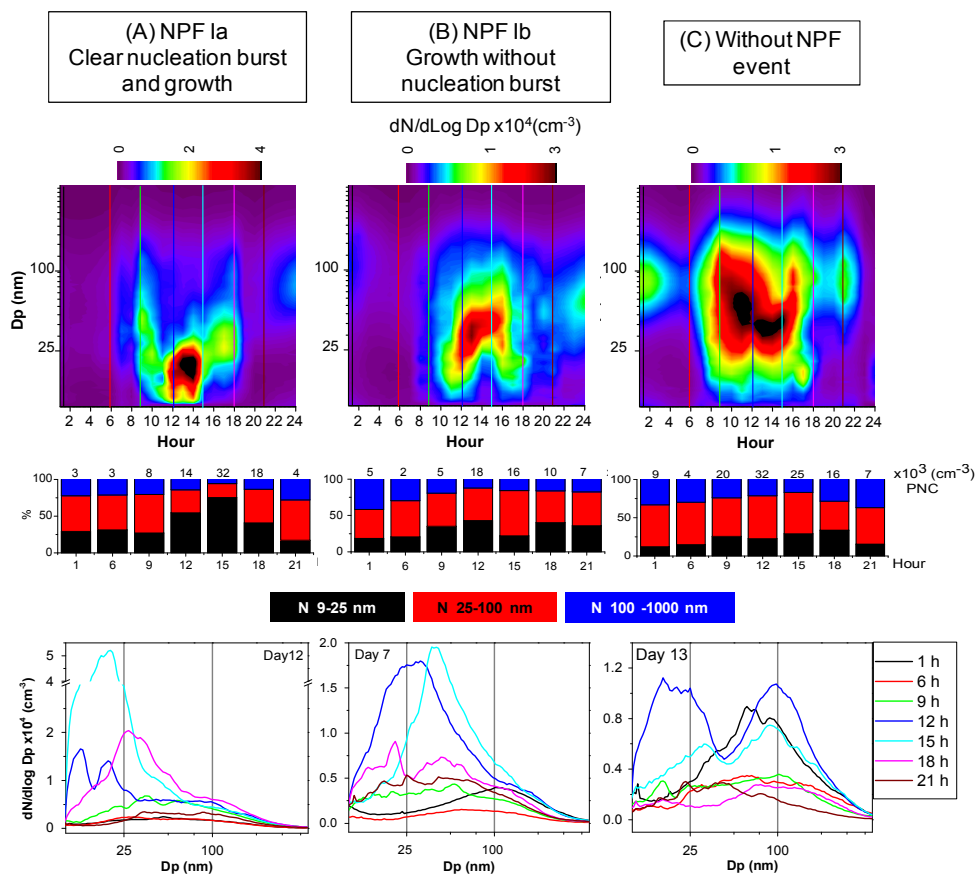
Figure 4. PND contour plots for days with (a) NPF Ia type, (b) NPF Ib type events and (c) without NPF event. The hourly bar show percentages of PNCs in three modes (nucleation, Aitken and accumulation) and hourly PND line graphs show PND distribution. Selected hours were marked on the PND contour in order to compare with the hourly PND graphs.
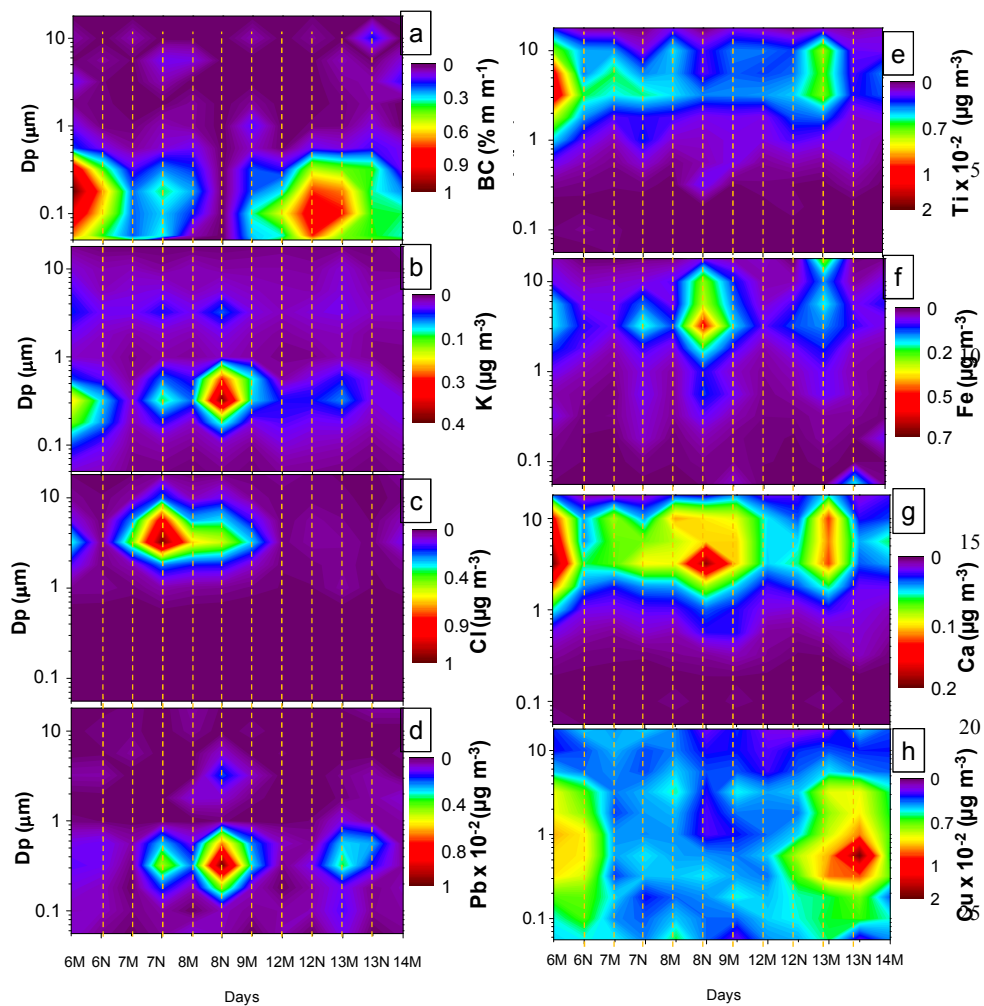
Figure 5. Mass size distribution of elemental concentrations of aerosol samples collected by MOUDI impactor (a–d and e–h)
during morning (0700–1800 h) and night (1900-0600 h), represented by M and N, respectively. All of these days are
weekdays.

29
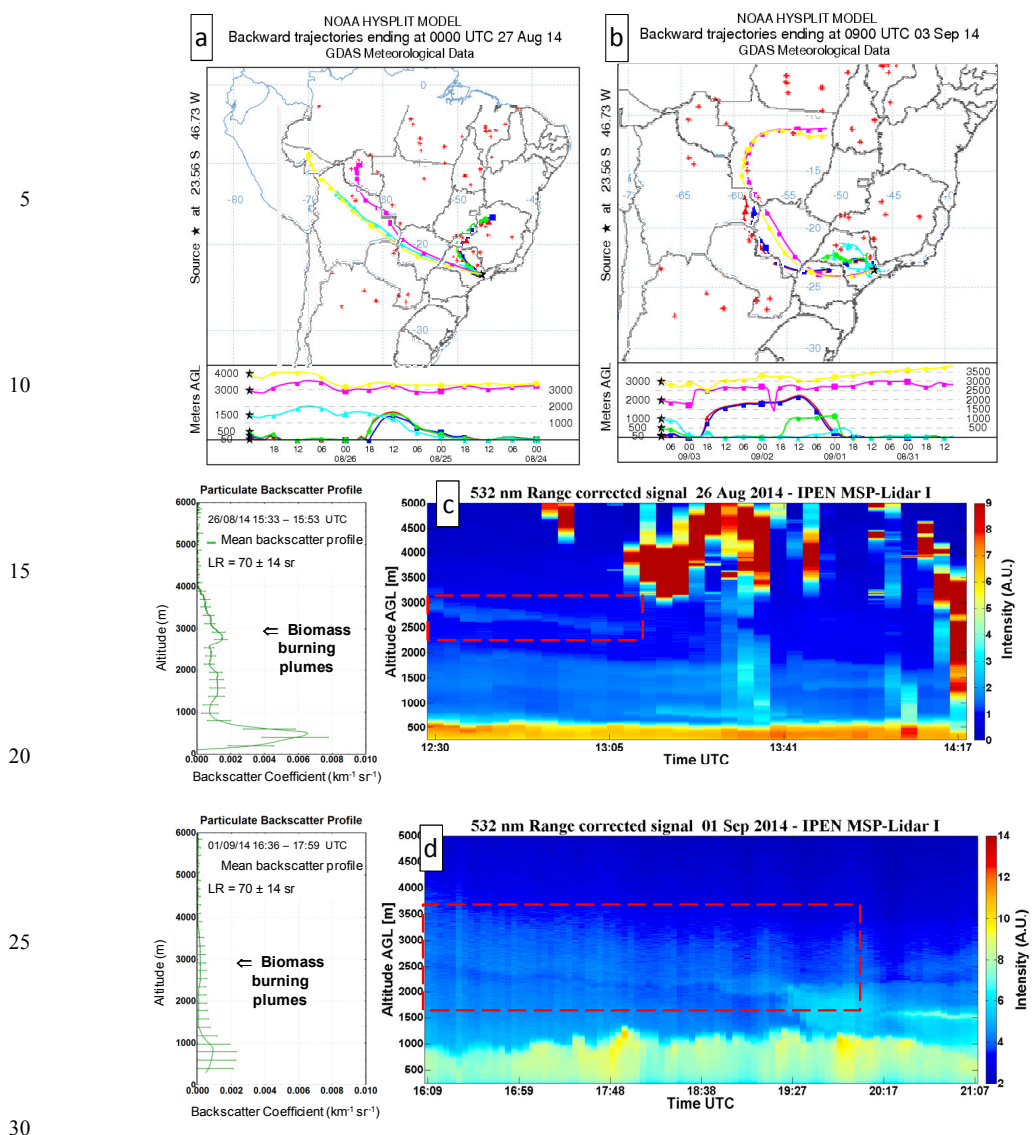
Figure 6. Trajectory and Lidar analyses for days with biomass burning events. The Hysplit trajectory models and biomass burning events for days 6, 7, 12, 13 and 14 are shown in figs. a and b. The particulate backscatter profile and Lidar analyses for days 6 and 12 are shown in figs. c and d. During these days the main wind trajectory was from north and northeast region, where predominates biomass burning events. The biomass burning plumes were detected by Lidar during these evaluated days and were also detected by GOES satellite (IPEN,2015).

Atmospheric
Chemistry
and Physics
Discussions
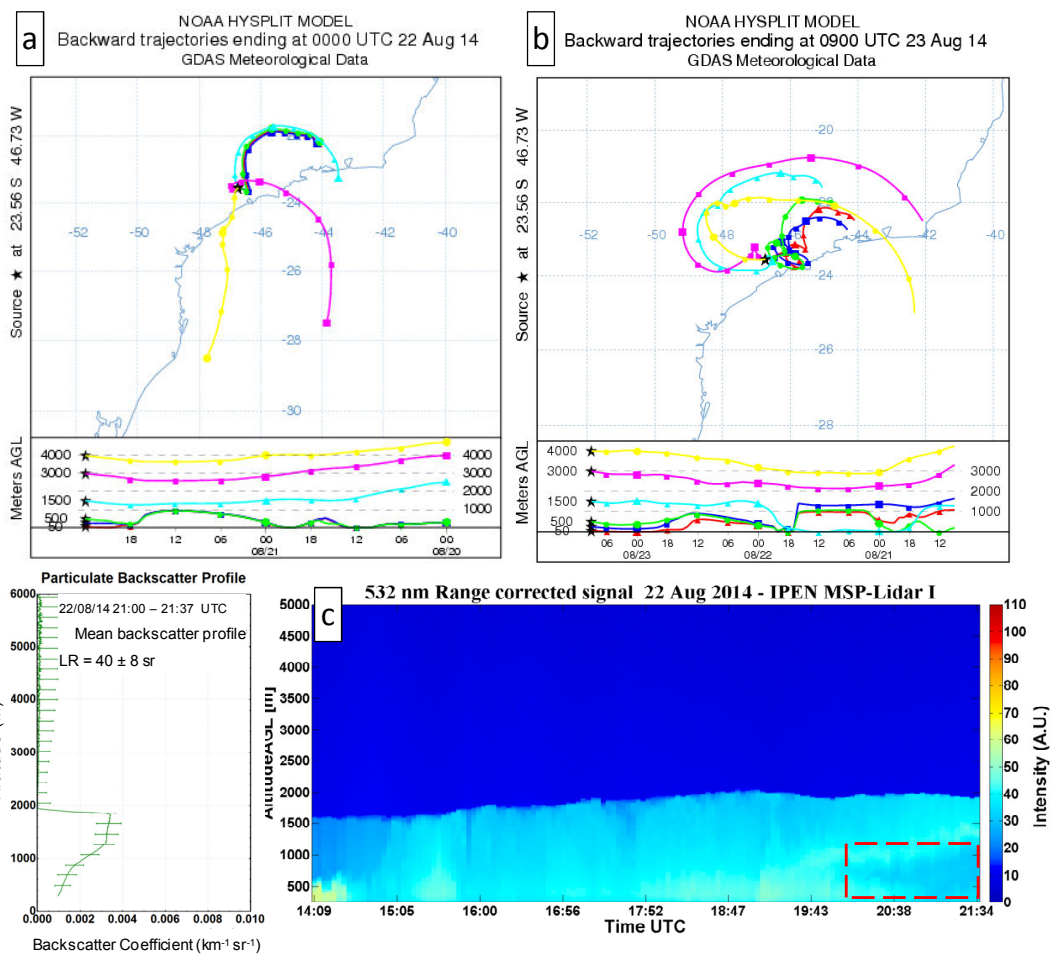
Figure 7. Trajectory and Lidar analyses for days with sea salt apportionment. The figures shown Hysplit trajectory models for days 3, 4, 5 (a,b) and also particulate backscatter profile and Lidar analyses for days 3 and 4 (c). During these days were observed main wind trajectory from south, southeast and southwest region, which is locate Atlantic Ocean and coastal region. The sea-salt plumes were detected by lidar analysis during day 4, while higher confidence interval (CI) concentrations were measured during days 7 and 8.

Atmospheric
Chemistry
and Physics
Discussions
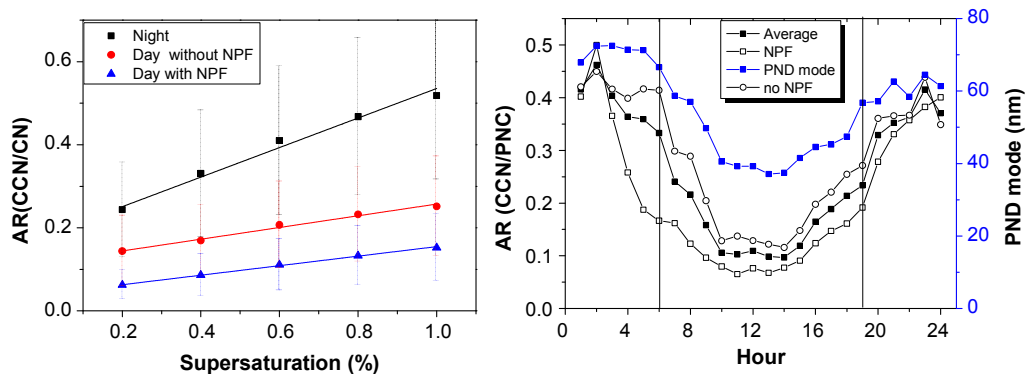
5

Figure 8. (a) Mean AR for diurnal, nocturnal and NPF events versus supersaturation. The difference between diurnal and nocturnal AR was mostly pronounced for SS higher than 0.6%.(b) Hourly average of AR for days without NPF and with NPF events. The AR values for nocturnal and diurnal showed clearly differences, while days with NPF events presented values slightly lower than days without NPF.
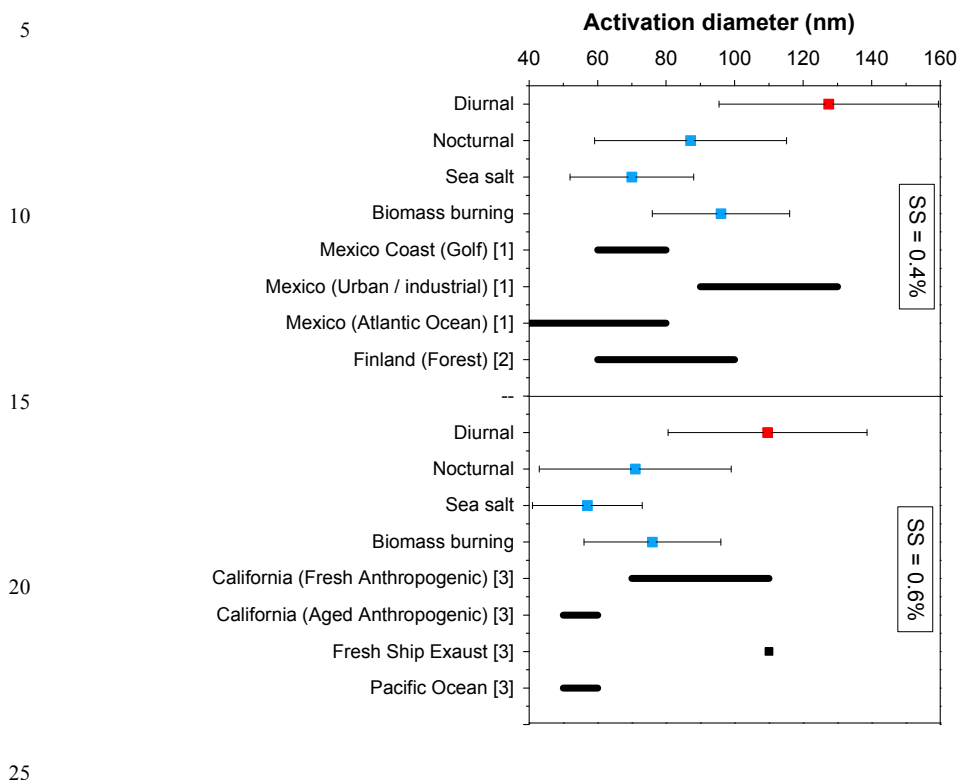
10

15

20
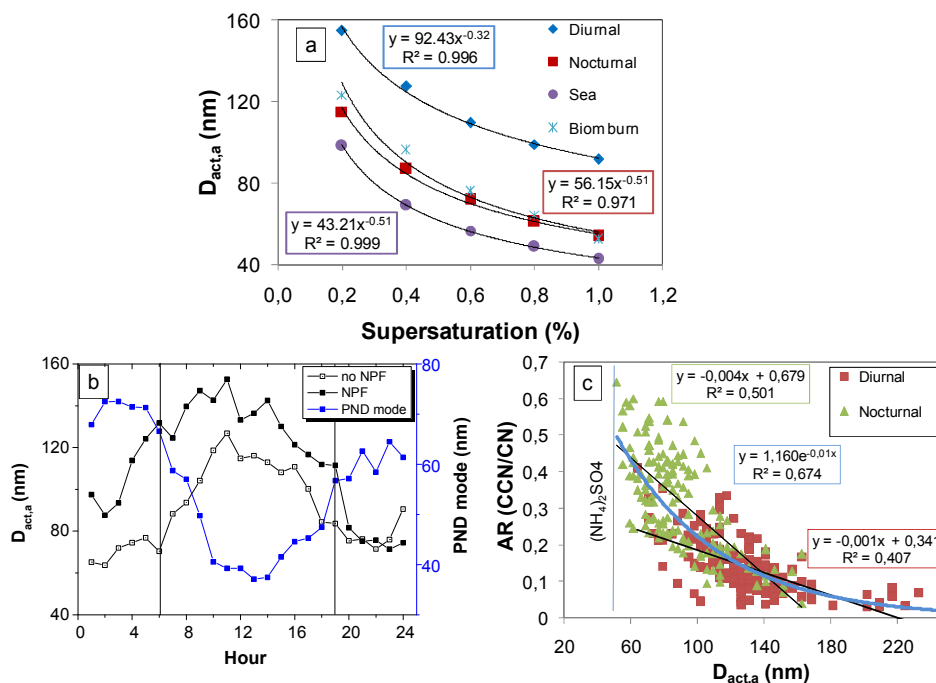
Figure 9. a) Apparent activation diameter ($D_{act,a}$) average for SS between 0.2 to 1.0%. b) Time series for days with and without NPF events c) Activated Ratio vs $D_{act,a}$. The $D_{act,a}$ were calculated for SS = 0.4%. This major $D_{act,a}$ increase occurred at lower supersaturation (SS < 0.2%).

5

10

15

Figure 10. Comparison of $D_{act,a}$ values obtained in this and previous studies from urban, coastal and forest environments. Sea salt and biomass burning averages were calculated for nocturnal periods that were confirmed air masses from these sources. [1] Quinn, et al.(2008), [2] Sihto et al.(2011), [3] Furutani et al.(2008).

5

10

15

20

25
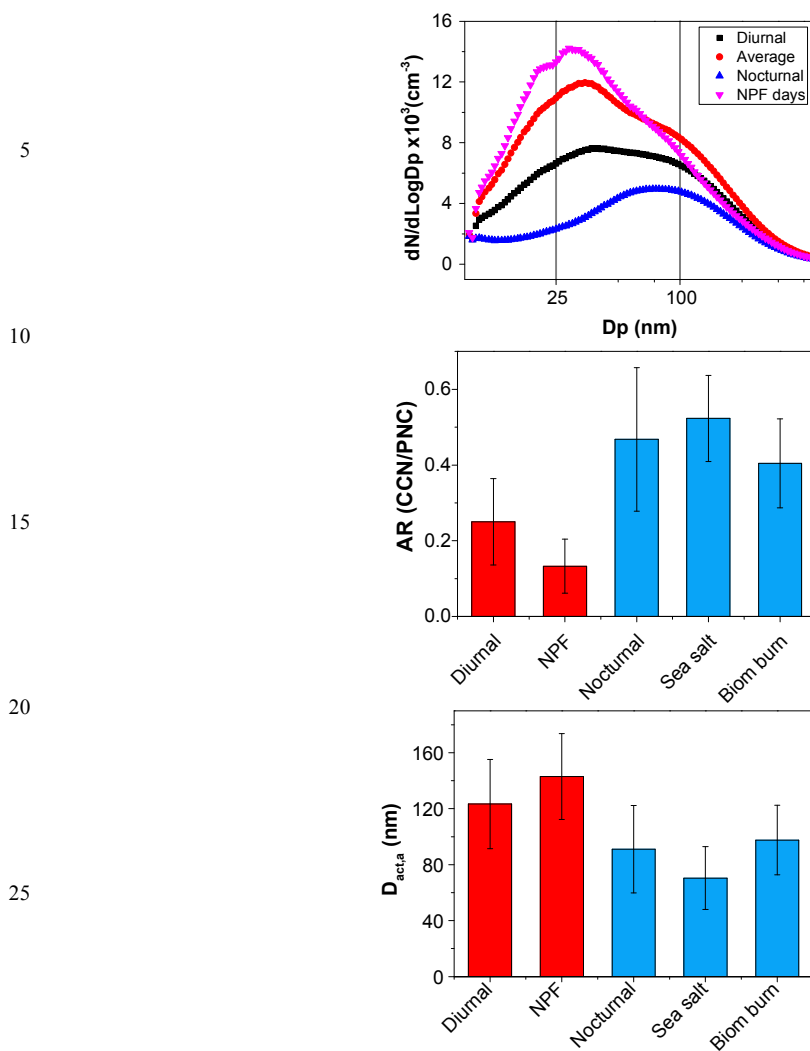
30

Figure 11. (a) Average diurnal and nocturnal particle size. Average of activated ratio (b) and diameter activation (c) for diurnal and nocturnal periods, as well during NPF, biomass burning and sea salt events.